

1 Measurement report: Atmospheric new particle formation in a peri- 2 urban site in Lille, Northern France

3 Suzanne Crumeyrolle¹, Jenni SS Kontkanen^{2,3}, Clémence Rose⁴, Alejandra Velasquez Garcia^{1,5}, Eric
4 Bourrienne¹, Maxime Catalfamo¹, Véronique Riffault⁵, Emmanuel Tison⁵, Joel Ferreira de Brito⁵, Nicolas
5 Visez⁶, Nicolas Ferlay¹, Frédérique Auriol¹, Isabelle Chiapello¹

6 ¹ Univ. Lille, CNRS, UMR 8518 Laboratoire d'Optique Atmosphérique (LOA), 59000 Lille, France

7 ² CSC - IT Center for Science, Espoo, Finland

8 ³ Institute for Atmospheric and Earth system Research, University of Helsinki, Helsinki, Finland

9 ⁴ Laboratoire de Météorologie Physique, LaMP-UMR 6016, CNRS, Université Clermont Auvergne, 63178, Aubière, France

10 ⁵ IMT Nord Europe, Institut Mines-Télécom, Univ. Lille, Centre for Energy and Environment, F-59000 Lille, France

11 ⁶Univ. Lille, CNRS, UMR 8516 - LASIRE - Laboratoire de Spectroscopie pour les Interactions, la Réactivité et
12 l'Environnement, F-59000 Lille, France.

13
14 *Correspondence to:* Suzanne Crumeyrolle (suzanne.crumeyrolle@univ-lille.fr)

15 Abstract.

16 Formation of Ultrafine particles (UFPs) in the urban atmosphere is expected to be less favored than in the
17 rural atmosphere due to the high existing particle surface area acting as a sink for newly-formed particles.
18 Despite the large ~~C~~ondensation ~~S~~ink (CS) values, previous comparative studies between rural and urban
19 site reported higher frequency of ~~N~~ew ~~P~~article ~~F~~ormation (NPF) events over urban sites in comparison to
20 background sites as well as higher particle formation and growth rates attributed to the higher
21 concentration of condensable species. The present study aims to better understand the environmental
22 factors favoring, or disfavoring, atmospheric NPF over Lille, a large city North of France and to analyze
23 their impact on particle number concentration using a ~~using a 4-year long-term dataset,~~
24 The results highlight a strong seasonal variation of the NPF occurrences with a maximum observed during
25 spring (27 events) and summer (53 events). It was found that high temperature ($T > 295\text{K}$), low RH ($\text{RH} <$

a supprimé: c

a supprimé: s

a supprimé: n

a supprimé: p

a supprimé: f

a supprimé: long-term dataset (4 years : 1st July 2017 to 31st December 2020). [f](#)

33 45, %) and high solar radiation are ideal to observe NPF events over Lille. Relatively high values of
34 condensation sink ($CS \sim 2 \cdot 10^{-2} \text{ s}^{-1}$) are reported during event days suggesting that high CS does not inhibit
35 the occurrence of NPF over our site. Moreover, the particle Growth Rate ($GR_{15.7-30\text{nm}}$) was positively
36 correlated with the temperature most probably linked to the higher emissions of precursors. Finally, the
37 nucleation strength factor (NSF) was calculated to highlight the impact of those NPF events on particle
38 number concentrations. $NSF_{15.7-100}$ reached a maximum of 4 in summer, indicating an enormous
39 contribution of NPF events to particle number concentration at this time of the year.

a supprimé: %

a supprimé: t

a supprimé: s

40 1 Introduction

41 New Particle Formation (NPF) leads to the formation of a large number of sub-20nm particles that will
42 contribute significantly to the levels of fine particles observed in ambient air. These particles can have
43 adverse effect on human health as they can penetrate deeply into the pulmonary system (Clifford et al.,
44 2018; Ohlwein et al., 2019). The freshly-formed particles then grow to larger sizes ($D_p > 100 \text{ nm}$) at
45 which they may act as cloud condensation nuclei (CCN, (Pierce and Adams, 2009; Ren et al., 2021; Rose
46 et al., 2017; Spracklen et al., 2006). NPF events have been observed around the world (Kerminen et al.,
47 2018; Kontkanen et al., 2017; Kulmala et al., 2004) in various environments from the boundary layer
48 (BL) at urban locations (Kanawade et al., 2022; Roig Rodelas et al., 2019; Tuch et al., 2006; Wehner and
49 Wiedensohler, 2003) as well as remote polar background areas (Dall'Osto et al., 2018) but also within
50 the free troposphere (Rose et al., 2015b, 2015a). NPF events are typically associated to a photochemical
51 origin, thus occurring mostly during daytime (Kulmala et al., 2014), with some scarce events being
52 observed during nighttime (Roig Rodelas et al., 2019; Salimi et al., 2017).

a supprimé: The latter

a supprimé: , from a few nm in particle diameter

a supprimé: up to sizes

53
54 NPF occurrence depends on various factors including precursor emission strength, number concentration
55 of pre-existing aerosol population, meteorological parameters (in particular solar radiation, temperature
56 and relative humidity) and oxidation capacity of the atmosphere (Kerminen et al., 2018). Differences were
57 found in both the seasonality and intensity of NPF events according to the site type (urban, traffic, regional
58 background, rural, polar, high altitude (Dall'Osto et al., 2018; Sellegri et al., 2019)). This variability seems

65 to be related to the environmental conditions that are specific to each location, which makes it hard to
66 draw general conclusions on the conditions that trigger NPF events (Berland et al., 2017; Bousiotis et al.,
67 2021). However, Nieminen et al. (2018) highlighted a common seasonal occurrence of NPF during spring
68 and summer using datasets from 36 continental sites worldwide.

69 The formation and growth of initial clusters to detectable sizes ($D_p > 1\text{-}3\text{ nm}$) compete with their
70 simultaneous removal from the ultra-fine particle mode by coagulation with pre-existing particles
71 (Kerminen et al., 2001; Kulmala, 2003). Because of this, the number concentration of particles smaller
72 than 20 nm has been observed to be anti-correlated with the aerosol volume and mass concentration over
73 rural area in Northern Italy (Rodríguez et al., 2005). Indeed, the total aerosol volume is rather small during
74 NPF events (Kerminen et al., 2018; Rodríguez et al., 2008). While the negative effect of increased pre-
75 existing particle surface area (often described with the condensation sink, CS) on the occurrence of these
76 events is widely accepted (Kalkavouras et al., 2017), yet cases are found when NPF events occur on days
77 with higher CS compared to average conditions (Größ et al., 2018; Kulmala et al., 2017).

78 A recent study (Bousiotis et al., 2021) used large datasets (16 sites) over Europe (6 countries) and
79 highlighted that solar radiation intensity, temperature, and atmospheric pressure had a positive
80 relationship with the occurrence of NPF events at the majority of sites (exceptions were found for the
81 southern sites), either promoting particle formation or increasing growth rate. Indeed, solar radiation is
82 considered one of the most important factors in the occurrence of NPF events, as it contributes to the
83 production of NPF precursors. Higher temperatures are considered favorable for the growth of newly
84 formed particles (Dada et al., 2017) as they can be linked to increased concentrations of organics vapor
85 (Wang et al., 2013) that support particle but also reduce the stability of the initial molecular clusters (Deng
86 et al., 2020; Kurtén et al., 2007).

87 The wind speed, on the other hand, has presented variable effects on the occurrence of NPF events results,
88 appearing to depend on the site location rather than their type (Bousiotis et al., 2021). Additionally, the
89 origin of the incoming air masses plays a very important role, since air masses of different origins have
90 different meteorological, physical and chemical characteristics. Therefore, the probability of NPF event
91 occurrence at a given location and time depends not only on local emissions, but also on long range

a mis en forme : Français

a supprimé: nucleation

a supprimé: ing

94 transport (Sogacheva et al., 2007, 2005; Tunved et al., 2006) and on synoptic meteorological conditions
95 at the European scale (Berland et al., 2017).
96 Formation of new particles in the urban atmosphere is expected to be less favored than in the rural
97 atmosphere due to the high existing surface area of particles acting as a sink for freshly-formed particles.
98 Despite the large CS values, previous comparative studies between rural and urban site reported higher
99 frequency of NPF events (Peng et al., 2017) over urban sites in comparison to background sites as well
100 as higher particle formation and growth rates (Nieminen et al., 2018; Salma et al., 2016; Wang et al.,
101 2017) attributed to the higher concentration of condensable species. This study presents the first
102 observations of new particle formations over Lille, a large city in the north of France. Based on a multi-
103 annual dataset (2017-2020), the frequency and intensity of the events are analyzed aiming to better
104 constrain the favorable and unfavorable conditions.

106 2 Materials and methods

107 The ATOLL (ATmospheric Observations in LiLLE) station is located in Villeneuve d'Ascq, Northern
108 France (50.6114 N, 3.1406 E, [60 m a.s.l.](#)), and only 4 km away from the city center of Lille, which is the
109 core of the metropolis (Métropole Européenne de Lille [with](#) more than 1.1 million inhabitants) to which
110 Villeneuve d'Ascq belongs. Observations such as low Single Scattering Albedo (SSA) values (0.75 on
111 average within the PM₁ fraction, Velasquez-Garcia et al., under review) and large particle number
112 concentrations (6140 cm⁻³ on average) suggest that aerosol measurements performed at ATOLL aerosol
113 conditions are comparable to [Global Atmospheric Watch](#) (GAW) sites classified as urban (Laj et al., 2020;
114 Rose et al., 2021). ATOLL is also part of ACTRIS (Aerosols, Clouds, and Trace gases Research
115 InfraStructure Network, <http://www.actris.net>) program, complementing the high-quality long-term
116 atmospheric data in Northern France. This station is under the influence of many anthropogenic sources,
117 e.g. road traffic, residential sector, agriculture and industries (Chen et al., 2022), as well as maritime
118 emissions, and more episodically under the influence of events of aged volcanic plumes and desert dust
119 (Boichu et al., 2019; Bovchaliuk et al., 2016; Mortier et al., 2013).

a supprimé: ,

121

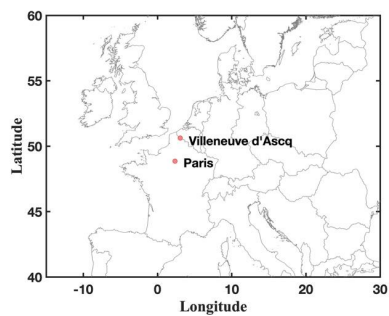


Figure 1 : ATOLL location in Villeneuve d'Ascq (Northern France) and picture of the station on the rooftop of the University of Lille P5 building (© LOA).

122

123 A large set of *in-situ* and remote sensing instruments are implemented in ATOLL to characterize physical,
124 chemical, optical and radiative properties of particles and clouds. *In-situ* instruments have independent
125 sampling stainless-steel lines located at least 1 meter above the roof top and equipped either with PM₁
126 cyclone or PM₁₀ inlet. The measurements used for that study were performed between 1st July 2017 and
127 31st December 2020. The instruments used in this study measure the aerosol properties including number,
128 size distributions, chemical composition, and optical properties. The details are described below.

129

130 The Scanning Mobility Particle Sizer (SMPS) measures particle number size distribution between 15.7-
131 800 nm downstream a Nafion membrane as recommended by ACTRIS standards to keep relative
132 humidity below 40%. The SMPS system consisted of a TSI model 3775 condensation particle counter, a
133 TSI 3081A₂-type differential mobility analyzer (DMA) as described by (Villani et al., 2007) and a Nickel
134 aerosol neutralizer (Ni-63 95MBq). The sheath flow rate was controlled with a critical orifice in a closed
135 loop arrangement (Jokinen and Mäkelä, 1997). The scan time was 300 seconds and the particle
136 concentrations were corrected by taking into account charge effects and diffusion losses given by the
137 manufacturer specifications (AIM 10.2.0.11).

a supprimé: The instruments use in this study focused on aerosol properties including number size distributions, chemical composition, and optical properties, and details are described below.

a supprimé: 2

a mis en forme : Police :Non Italique

a supprimé: Typically, the scan time was chosen to be 300 seconds. To take into account the multiple charge effect and the losses through diffusion, particle concentrations were corrected using the equation ...

146 Accordingly, aerosol number size distribution data from the SMPS measurements were used to classify
 147 individual days as NPF event, undefined or non-event days. The classification procedure, presented in
 148 Dal Maso et al. (2005), is following the decision criteria based on the presence of fine particles ($D_p < 25$
 149 nm) and their consequent growth to Aitken mode ($D_p < 80$ nm). Briefly, event days are identified when
 150 sub-25nm particle formation and growth are observed. On non-event days nucleation mode is absent.
 151 Finally, undefined days are the days when sub-25nm particles are observed but do not grow subsequently
 152 or last less than an hour.

153 SMPS particle number size distributions were also used for CS ($CS = 2\pi D \sum_i \beta_{Mi} d_{pi} N_i$)
 154 Equation 1, where β_{Mi} is the transitional correction
 155 factor (Fuks and Sutugin, 1970), the Knudsen number is $Kn = 2\lambda_v / d_p$, and α is the accommodation
 156 coefficient and set to unity here) and GR calculations. The CS estimates the loss rate of the condensable
 157 vapors (Kulmala et al., 2001), which were assumed to have molecular properties similar to sulfuric acid
 158 for CS calculation (Dal Maso et al., 2005). A high CS indicates the presence of large surface area of
 159 aerosol particles onto which NPF precursors can condensate. The particle GR_{15.7-30} from 15.7 to 30nm,
 160 was calculated based on the maximum-concentration method described in (Kulmala et al., 2012). First,
 161 the NPF starting time was identified when the newly formed mode was observable in the first bin of the
 162 SMPS (15.7 nm). Then, the time when the concentrations for particles with diameter of 30 nm (N_{30})
 163 peaked, was also manually identified. Particle GR_{15.7-30} was then calculated by linear regression of particle
 164 size vs. time span from the NPF start until time when N_{30} reaches a maximum ($GR = (D_{p,2} - D_{p,1}) / T2 -$
 165 $T1$).

167 $CS = 2\pi D \sum_i \beta_{Mi} d_{pi} N_i$ Equation 1

168 $\beta_{Mi} = \frac{1 + Kn}{1 + 0.337Kn + \frac{4}{3}\alpha^{-1}Kn + \frac{4}{3}\alpha^{-1}Kn^2}$ Equation 2

169
 170 Absorption coefficients (σ_{abs}) were continuously measured with a seven-wavelength aethalometer (AE33,
 171 Magee Scientific Inc., Cuesta-Mosquera et al., 2020). According to ACTRIS current guidelines

a supprimé: followed the procedure... presented in Dal Maso et al. (2005), (Dal Maso et al., 2005) ... [1]

a supprimé: dry (using a Nafion)
 a mis en forme : Police : Gras
 a mis en forme ... [2]

a supprimé: growth rate (...R) ... [3]

a mis en forme : Non souligné

a supprimé: (Fuks and Sutugin, 1970)... high CS indicates the presence of large surface area of aerosol particles onto which NPF precursors can condensate and particles can coagulate as well... The particle GR_{15.7-30}GR... from 15.7 to 30nm, was calculated based on the maximum-concentration method described in (Kulmala et al., 2012). First, the NPF starting time was identified when the newly formed mode was observable in the first bins... of the SMPS (15.7 nm), and ...then, the time of ...hen the peak ...concentrations for particles with diameter of 30 nm (N_{30}) peaked during NPF ...as alsoere ... [4]

a mis en forme : Police : 12 pt
 a mis en forme ... [5]

a mis en forme ... [6]

a mis en forme : Couleur de police : Automatique, Anglais (G.B.)
 a mis en forme : Bordure : Haut: (Pas de bordure), Bas: (Pas de bordure), Gauche: (Pas de bordure), Droite: (Pas de bordure), Entre: (Pas de bordure), Motif : Transparente

(https://actris-ecac.eu/particle-light-absorption.html), σ_{abs} coefficients at each wavelength have been recalculated by 1) multiplying equivalent Black Carbon (eBC) by the mass-specific absorption coefficient (MAC) and then 2) dividing by the suitable harmonization factor to account for the filter multiple scattering effect, i.e. 2.21 (M8020 filter tape) in 2017 and 1.76 (M8060 filter tape) afterwards. The aethalometer samples at 5 L_{min}⁻¹ downstream a PM₁ cyclone (BGI SCC1.197, Mesa Labs). The spectral dependency of σ_{abs} was used to determine the contributions of traffic (fossil fuel - FF) and Wood Burning (WB) to eBC via a source apportionment model (Sandradewi et al., 2008). Meteorological data including temperature, water vapour mixing ratio, and solar radiation were also measured every minute at the sampling site using a weather station (DAVIS Inc weather station, Vantage Pro 2) and a set of Kipp and Zonen pyranometer (CM22) and pyrheliometer (CH1). A skyimager (Cloudcam, CMS) was also used to estimate the sky cloudiness (Shukla et al., 2016). Three-day air mass backtrajectories of air masses arriving at ATOLL at half the boundary layer height between July 1, 2017 and December 31, 2020 were computed every hour using the Hybrid Single-Particle Lagrangian Integrated Trajectory (HYSPLIT version 5.1.0) transport and dispersion model from the NOAA Air Resources Laboratory (ARL) (Rolph et al., 2017; Stein et al., 2015) and meteorological input from the Global Data Assimilation System (GDAS) at 1×1° resolution, resulting in 30719 backtrajectories.

3 Results

3.1 NPF event frequency

The seasonal distribution of NPF events at the ATOLL site is displayed in Figure 2. SMPS missing data (in Figure 2) are about 40% from January to April due to the yearly calibrations at the manufacturer premises and few laboratory campaigns (Oct 2018 – Jun 2019). Over the 4 years of measurements (2017-2020), 96 (11%) days were classified as NPF events, 355 (40%) as undefined days and 432 (49%) as non-event days. One can also note that most of the NPF events identified at the ATOLL site were observed during spring (March-April-May, 27 events corresponding to 15% of the days when observations were available during this season) and summer (June-July-August, 53 events corresponding to 19%) with a

a supprimé: .

a supprimé: .

a supprimé: and pyrgeometer (CGR4).

a supprimé: and Growth rate

a supprimé: %

a supprimé: %

a supprimé: %

a supprimé: %

a supprimé: %

a supprimé: %

236 maximum observed in June consistent with a previous study over central Europe (Dall'Osto et al., 2018).
237 During winter, the number of events is extremely limited (only one event observed in February). In the
238 following sections, only observations from spring and summer seasons will be discussed due to the low
239 representativeness of NPF events in fall (n=15) and winter (n=1). Moreover, the undefined event days are
240 seen all year round (frequency around or larger than 20,%) with a clear peak in August (frequency at 62.5,
241 %) consistent with observations over boreal forest where undefined days were also observed to be most
242 frequent in early fall (Mazon et al., 2009).

243 Using long-term measurements from 36 sites (polar, rural, high altitude, remote and urban), Nieminen et
244 al., (2018) reported an annual NPF frequency below 15, % for half of the sites (18 sites from all types)
245 and occasionally over 30, % for 10 sites. Moreover, they highlighted a seasonal variation of NPF
246 occurrence with larger (lower) frequency, about 30, % (10, %), during spring (winter). Frequency analysis
247 of NPF occurring only over urban or anthropogenically influenced sites show large site-to-site differences
248 for all seasons. Indeed, NPF occurrence frequencies are varying from 20, % (Helsinki in Finland, Sao
249 Paulo in Brazil) to 80, % (Beijing in China, Marikana in South Africa) during spring and from 7, %
250 (Helsinki) to 78, % (Marikana) during winter. Yearly average of NPF occurrence frequencies are between
251 11, % (Helsinki) and more than 60, % (Beijing and Marikana).

252

253 The ATOLL event frequency (seasonal variation and values) is similar to observations performed in Paris
254 (Dos Santos et al., 2015) while the frequency of undefined and non-event days are quite different. Indeed,
255 in Paris the non-event frequency is larger than 60, % except in July and August whereas over ATOLL the
256 non-event frequency shows a clear seasonal pattern with lower frequency (<40, %) from April to August.
257 Moreover, undefined event frequency in Paris shows a minimum (<5, %) in May and June and remains
258 quite steady during the rest of the year (around 20, %). One can note that the frequency of undefined events
259 (also considered as failed events) is much higher over ATOLL all year long with an average of 40, %
260 while it remains below 40, % over the boreal forest. The frequency of undefined events observed at
261 ATOLL is clearly larger than the frequencies observed over more polluted site (Paris) and a pristine site
262 (Boreal forest). This might show that ATOLL is under the influence of air masses or particle and precursor
263 sinks that favor the burst of UFP.

a supprimé: %
a supprimé: %

a supprimé: ,
a supprimé: %
a supprimé: %
a supprimé: %
a supprimé: %

a supprimé: %
a supprimé: %
a supprimé: %
a supprimé: %
a supprimé: %

a supprimé: %
a supprimé: %
a supprimé: %
a supprimé: %
a supprimé: %
a supprimé: %

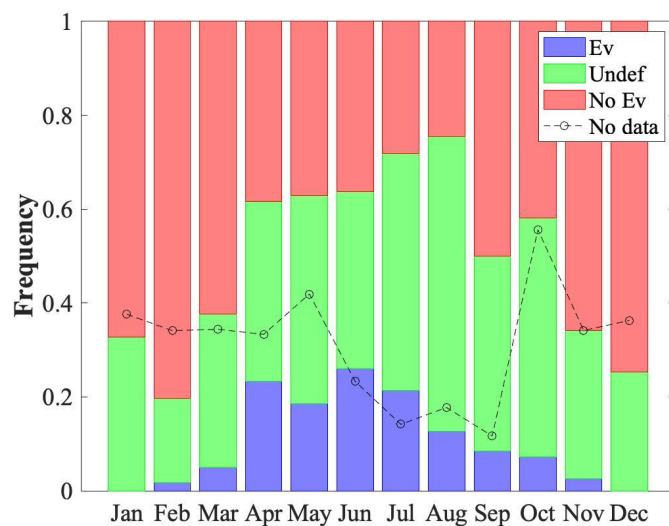


Figure 2 : Seasonal distribution of event days (blue), undefined days (green), and non-event (red) days at the ATOLL station, Lille, France, during 2017–2020. Days with missing data are excluded from the total number of days per month and the frequency of missing data are indicated with the black circles.

3.2 Aerosol number size distribution

Median daily contour plots of the particle number size distributions (PNSD) obtained from the SMPS are shown in Figure 3 separately for NPF event (around 800 PNSD), undefined (around 2300 PNSD) and non-event (around 1700 PNSD) days observed during the warm period (only spring and summer). The PNSD were first selected then averaged to one-hour time resolution using median filtering. Atmospheric

a supprimé: dry

a déplacé vers le bas [3]: Median daily contour plots of the particle number size distributions (PNSD) obtained from the SMPS are shown in Figure 3 separately for NPF event, undefined and non-event days observed during the warm period (only spring and summer). Median daily contour plots of the

a déplacé (et inséré) [3]

a mis en forme : Couleur de police : Automatique

a mis en forme : Police : (Par défaut) Times New Roman, Couleur de police : Automatique

a mis en forme : Anglais (E.U.)

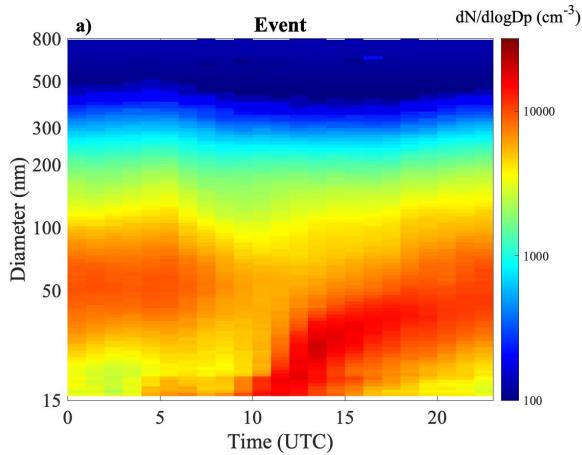
a mis en forme : Anglais (E.U.)

a mis en forme : Anglais (E.U.)

a mis en forme : Anglais (E.U.)

297 NPF and subsequent particle growth are seen in Figure 3a as an emergence of new aerosol particles with
298 small diameter followed by the growth of these particles into larger sizes. If this phenomenon is taking
299 place regionally (few tens of km in radius), a so called ‘banana plot’ is observed in particle number size
300 distributions as a function of time at a fixed location. The time evolution of the “median NPF day” (Figure
301 3a) displays a similar growth pattern for newly formed particles than for individual NPF event days (see
302 supplementary materials). Indeed, one can clearly see a UFP mode appearing from 10:00 to 15:00 (UTC)
303 and growing during the rest of the day. The NPF starting time and the growth rate will be discussed in the
304 following section. By 23:00 UTC, the newly formed particles reach an average diameter of 50 nm, similar
305 to the median diameter of the mode of the pre-existing particles observed during the morning (00:00 –
306 08:00). The “median undefined day” (Figure 3b) highlights a burst of UFP from 10:00 to 15:00 (UTC)
307 that is not growing and does not last during the whole afternoon. The behavior of the median is again
308 similar to the individual undefined events observed during this period. The “median non-event day”
309 (Figure 3c) shows no sign of particle growth, as expected.

310
311



a supprimé: s

a supprimé: geometric

a mis en forme : Couleur de police : Automatique

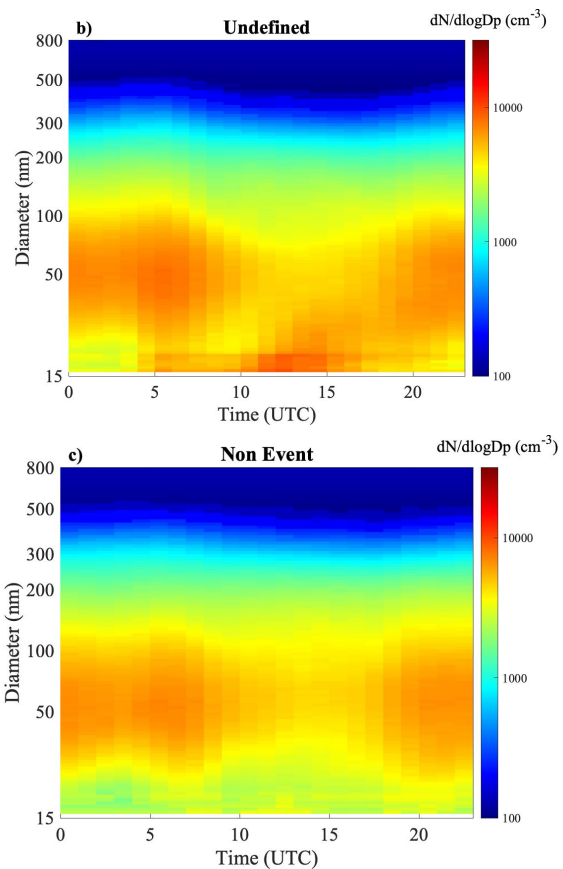


Figure 3 : Hourly median particle number size distribution ($15.7 \text{ nm} < D_p < 800 \text{ nm}$) observed during NPF event (a), undefined (b) and non-event (c) days in spring and summer from 2017-2020.

a supprimé: M

316 3.3 NPF starting time and growth rate

317 Figure 4 shows the monthly variation of the starting time and growth rate of each event observed at

318 ATOLL. Most NPF events observed in ATOLL were observed to start between 09:00 and 14:00 UTC

319 (74 %), with fewer events starting in the early morning (07:30 – 09:00 UTC, 6 %) and late afternoon

320 (15:00 and 19:30, 20 %). NPF starting time as well as $GR_{15,7-30nm}$ strongly depend on the month during

321 which the event is observed. Indeed, the NPF starting time is later during spring (also true for fall and

322 winter) and reaches a minimum in June (around 08:20). Nocturnal events are rarely observed, with only

323 one occurrence in August. No diurnal NPF event were observed after 16:00 UTC in summer. During

324 spring and fall, the average NPF starting time varies between 10:00 and 19:00 UTC. The start time

325 monthly variability is linked to sunrise and sunset times. In the following section, a link between the total

326 solar irradiation and NPF occurrence will be examined.

327 The event ending time was determined as the time when the growth of the freshly formed particles was

328 over, i.e. when the diameter reached the diameter of the pre-existing particles. The duration of nucleation

329 events, at ATOLL, was then estimated and varies from an hour up to 28 hours. On average, NPF duration

330 is shorter from May to August (around 8 hours) and increases up to around 13 hours on average during

331 March and November. This seasonal behavior could be due to the presence of availability of condensable

332 vapors, air mass origin, and environmental conditions favorable to NPF events (see section 3.2).

333

334

- a supprimé: S
- a supprimé: Growth
- a supprimé: local time
- a supprimé: %
- a supprimé: -
- a supprimé: %
- a supprimé: %
- a supprimé: GR
- a déplacé (et inséré) [1]
- a supprimé: Indeed, the NPF starting time becomes earlier during the colder period and reaches a minimum in June (around 08:20).
- a déplacé vers le haut [1]: Nocturnal events are rarely observed, with only one occurrence in August.
- a supprimé: colder months (
- a supprimé:)

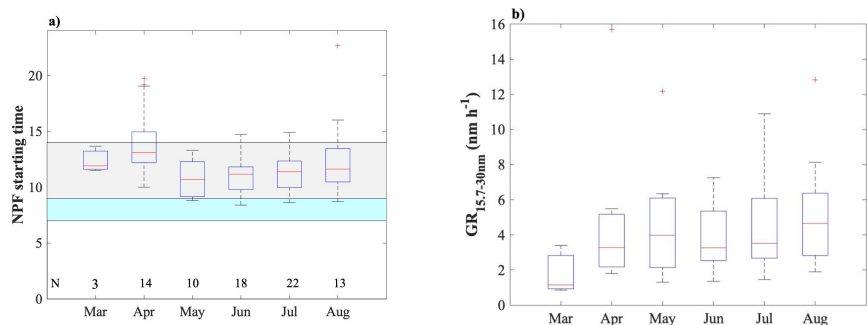


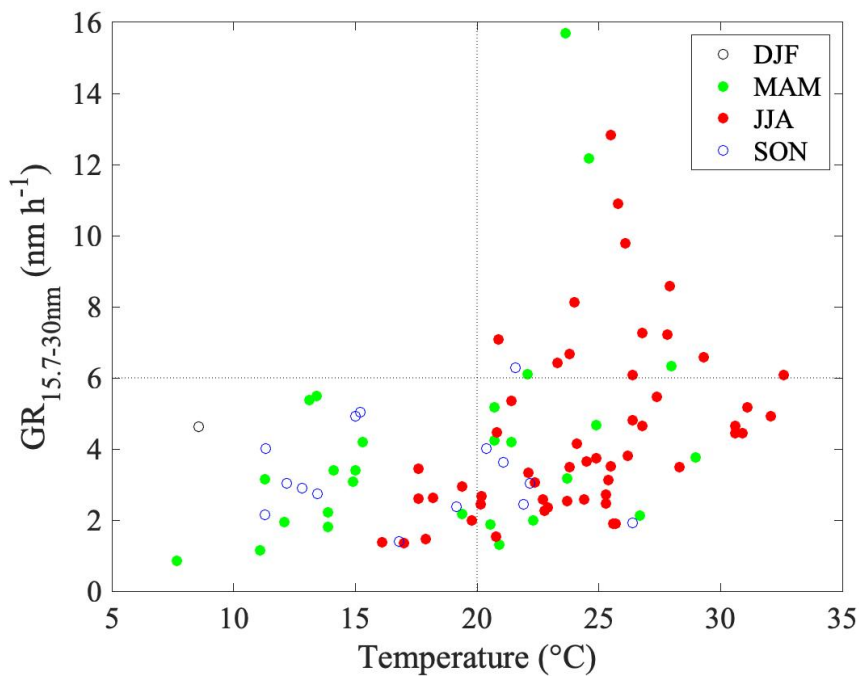
Figure 4 : Monthly variation of new particle formation starting time (a) and their Growth Rate ($GR_{15.7-30nm}$) at the ATOLL station during 2017–2020. The grey area represents the period, from 09:00-14:00, when most of the NPF events occur. The blue area corresponds to the period before the NPF onset (07:00- 09:00). N represents the number of events observed per month.

a mis en forme : Espace Après : 10 pt, Bordure : Haut: (Pas de bordure), Bas: (Pas de bordure), Gauche: (Pas de bordure), Droite: (Pas de bordure), Entre : (Pas de bordure)

a mis en forme : Police :9 pt, Gras

The Growth Rate ($GR_{15.7-30nm}$) values observed at ATOLL lie within 0.8 to 15.7 $nm \cdot h^{-1}$ and show a strong monthly variation with the lowest values observed in spring and fall and the largest ones observed during summer (Figure 4). $GR_{15.7-30nm}$ values were in addition plotted as a function of temperature for all years and seasons in Figure 5, which highlights that below 20°C, $GR_{15.7-30nm}$ values are lower than 6 $nm \cdot h^{-1}$, while, under warmer conditions ($T > 20^\circ C$), $GR_{15.7-30nm}$ reach values up to 16 $nm \cdot h^{-1}$. These results show a clear temperature dependence of the particle growth. Indeed, higher temperatures have been shown to favor emission of biogenic precursors, including monoterpenes known to favor the occurrence of NPF events (Kulmala et al., 2004). Previous studies (Paasonen et al., 2018; Yli-Juuti et al., 2011) have shown that the growth rate usually has larger values during warm periods and especially during summer. Over urban areas such as Beijing or Shanghai, $GR_{15-25nm}$ showed no clear seasonal variation (Yao et al., 2018). However, recent studies also have highlighted the link with growth rate seasonal pattern and high abundance of biogenic volatile organic compounds during warmer periods (spring and summer) over boreal forest (Paasonen et al., 2018; Yli-Juuti et al., 2011). Therefore, the observed seasonal variation of

363 GR_{15.7-30nm} values may be related to temperature variation that influences the emissions of organic
364 compounds in the atmosphere (Figure 5).
365 As previously observed in Figure 3a, the median diameters reached by the end of all NPF events are
366 similar and averaged around 50 nm. Moreover, the seasonal variation of the NPF event duration could be,
367 then, linked to the GR_{15.7-30nm} seasonal variation. As the final diameter is similar in all cases, the lower
368 the GR_{15.7-30nm} values will then be associated with the longer NPF duration. The seasonal variation of
369 NPF duration highlighted earlier could then only be a consequence of the GR_{15.7-30nm} seasonal variation.
370



371 Figure 5 : Growth Rate (GR_{15.7-30nm}) values as a function of ambient temperature.

a mis en forme le tableau

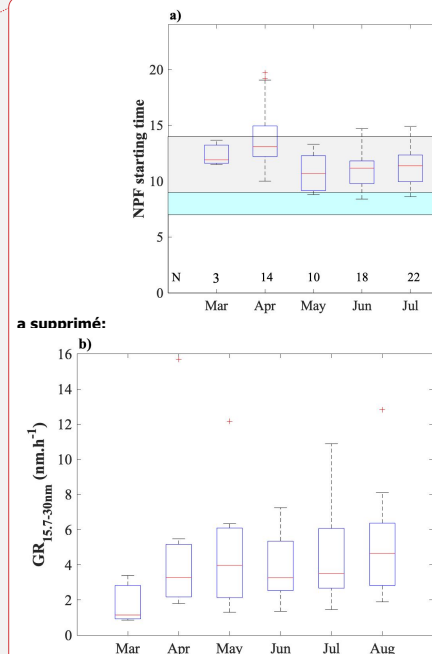
a mis en forme : Retrait : Première ligne : 1,27 cm

372
373
374

3.4 Environmental conditions

375 The effect of cloudiness on NPF event occurrence is shown in Figure 6a, with a specific focus on
376 measurements collected between 09:00 and 14:00, i.e. the period of time where most NPF tended to start.
377 The cloud fraction was calculated from the sky imager dataset following the method by (Shukla et al.,
378 2016) and sorted as a function of event, undefined and non-event days. There is a clear inverse correlation
379 between cloud fraction and NPF occurrences. Average cloud fraction is around 0.47 during event days,
380 0.68 during undefined days and 0.74 during non-event days. Moreover, the 25th percentiles of the cloud
381 fractions for event, undefined and non-event days, respectively 0.06, 0.47, 0.63, clearly show that the
382 absence of clouds (lower cloud fraction) is mostly associated with NPF events. This result is consistent
383 with previous analysis performed over the boreal forest (Dada et al., 2017) and is linked to the fact that
384 radiation seems essential for NPF during the warmer period ([spring and summer](#)), as the events occur
385 almost solely during daylight hours (Kulmala et al., 2004). Figure 6b shows the average diel total solar
386 radiation, observed during events, non-event and undefined days for spring and summer. As expected,
387 total solar radiation is on average always larger during event days in comparison to non-event days, with
388 a more pronounced difference observed during spring.

389



a supprimé:

Figure 4 : Monthly variation of new particle formation starting time (a) and their Growth Rate ($GR_{15.7-30nm}$) at the ATOLL station during 2017–2020. The grey area represents the period, from 09:00-14:00, when most of the NPF events occur. The blue area corresponds to the period before the NPF onset (07:00- 09:00). N represents the number of events observed per month.

The growth rate values ($GR_{15.7-30nm}$) observed at ATOLL lie within 0.8 to 15.7 $nm.h^{-1}$ and show a strong monthly variation with the lowest values observed in spring and fall and the largest ones observed during summer (Figure 4). $GR_{15.7-30nm}$ values were in addition plotted as a function of temperature for all years and seasons in Figure 5, which highlights that below 20°C, $GR_{15.7-30nm}$ values are lower than 6 $nm.h^{-1}$, while, under warmer conditions ($T > 20^\circ C$), $GR_{15.7-30nm}$ reach values up to 16 $nm.h^{-1}$. These results show a clear temperature dependence of the particle growth. Indeed, higher temperatures have been shown to ... [7]

a supprimé: s

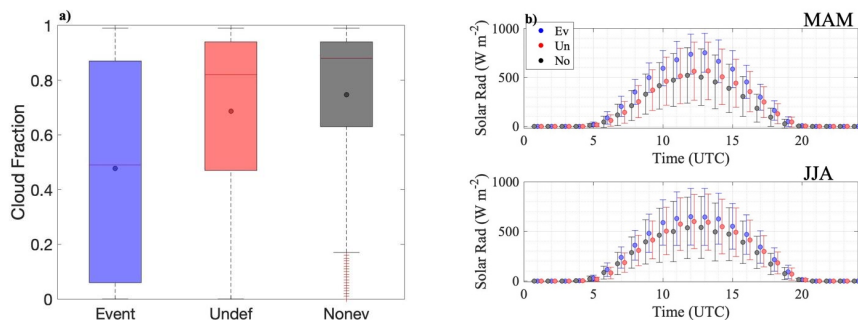
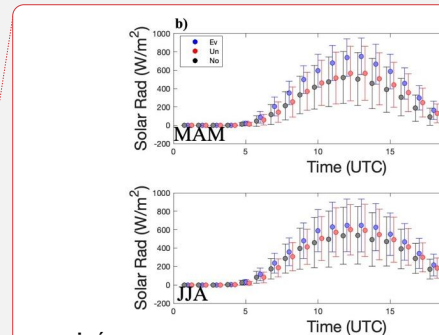


Figure 6 : (a) Cloud fraction observed from 09:00 to 14:00 UTC during event, undefined and non-event days. The red line represents the median while the lower and upper edges of the box represent the 25th and 75th percentiles, respectively. The lower and upper edges of the whisker represent 10th and 90th percentiles, respectively. The circles represent the average. (b) Diel variations (UTC) of the mean total solar radiation observed during the event days (blue), undefined days (green) and non-event days (red) during spring (MAM, top) and summer (JJA, bottom) seasons (b). The error bars correspond to one standard deviation.



a supprimé:

Other environmental parameters known to influence the occurrence of NPF events, such as temperature and humidity were also sorted to highlight diel and seasonal variations (Figure 7). Our results (Figure 7a) indicate that NPF is favored by low values of ambient relative humidity, especially during spring, consistently with previous studies (Duplissy et al., 2016; Hamed et al., 2011; Merikanto et al., 2016). A few reasons can explain this tendency: (1) high RH values ($RH > 90\%$) observed at the surface are usually associated to the presence of low altitude clouds reducing incoming total radiation and then preventing NPF formation, (2) at moderately high RH ($RH > 40\%$), hydrophilic aerosols could grow which will enlarge the sink for precursors and (3) high RH values limit some VOC (Volatile Organic Compounds) ozonolysis reactions, which further prevents the formation of condensable vapors necessary for nucleation (Boy and Kulmala, 2002).

Figure 7b shows the diel median temperature conditions (T) during NPF events, nonevents and undefined days. NPF events occurred within temperatures ranging between 3°C and 33.5°C. During both seasons, averaged temperatures during event days are always larger than during non-event days, with, again larger

a supprimé: %

a supprimé: %

a supprimé: th

466 differences during spring. One should note that days with high temperatures in spring and summer are
 467 usually also days with high solar radiation, consistently with conclusions from Figure 6. The temperature
 468 difference between undefined days and event days is clearly marked during spring and fade away during
 469 summer. As previously discussed, higher temperatures favor emission of biogenic precursors, including
 470 monoterpenes known to favor the occurrence of NPF event (Kulmala et al., 2004). Isoprene emission is
 471 also favor at higher temperature but according to (Heinritzi et al., 2020) its presence can make the
 472 difference between measurable new-particle formation events and their absence. Moreover, high
 473 temperature can also lead to evaporation of molecular clusters which may inhibit NPF events (Dada et
 474 al., 2017; Deng et al., 2020).

475

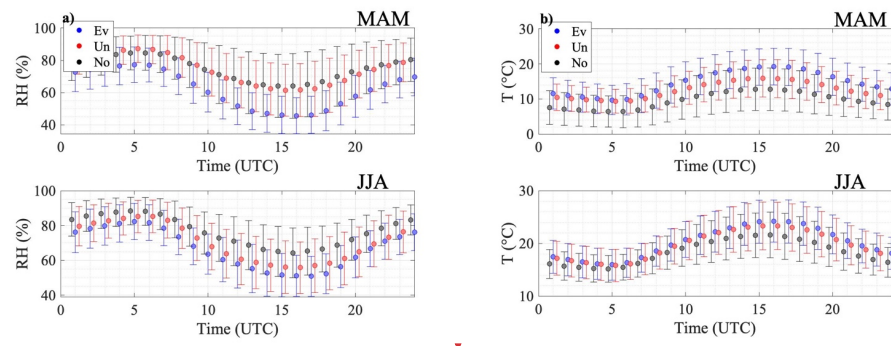


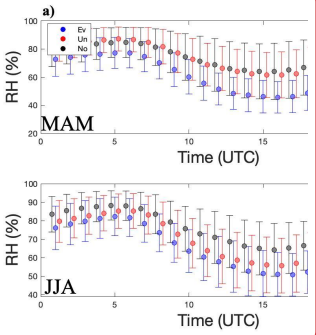
Figure 7 : Diel variation (UTC) of mean Relative Humidity (RH, a) and mean temperature (b) observed during the event days (blue), undefined days (green) and non-event days (red) during spring (MAM) and summer (JJA) seasons. The error bars correspond to one standard deviation.

476 **3.5 Condensation sink**

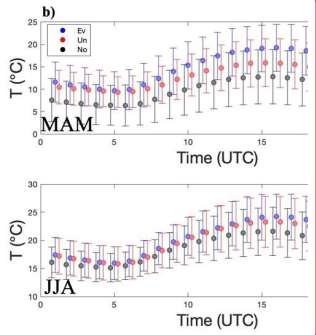
477 The CS characterizes the loss rate of atmospheric vapors to aerosol particles. The diel variations of CS
 478 calculated for spring and summer and for NPF event, undefined and non-event days are shown in Figure
 479 8a. Averaged CS values are high (larger than $2 \cdot 10^{-2} \text{ s}^{-1}$) during event days occurring during spring and

a supprimé: (Heinritzi et al., 2020). However

a mis en forme : Couleur de police : Automatique, Anglais (E.U.)



a supprimé:



a supprimé:

a mis en forme : Justifié, Interligne : 1,5 ligne

a supprimé:

484 summer (Figure 8a). During NPF event days and over different urban sites (Beijing, Nanjing or Hong
485 Kong), CS values ranging from 0.6 up to $10.7 \cdot 10^{-2} \text{ s}^{-1}$ were reported (Xiao et al., 2015). Over pristine sites,
486 such as Hyytiälä, the CS values are between $0.05 - 0.35 \cdot 10^{-2} \text{ s}^{-1}$. As events occur anyway, low values of
487 CS, often considered as the major limiting factor in the NPF occurrence do not inhibit the occurrence of
488 NPF events in ATOLL consistently to previous observations in similar environments, such as Melpitz
489 observatory (Größ et al., 2018) or over Chinese megacities (Xiao et al., 2015). One can assume that the
490 presence of large concentrations of precursors could explain the formation of particles over polluted sites
491 such as ATOLL. Unfortunately, precursors were not measured over the 4-year period of interest here
492 therefore this assumption would require further investigation beyond the scope of this study. Recent
493 studies (Marten et al., 2022; Wang et al., 2020), performed in the CLOUD chamber, demonstrates that
494 the presence of nitric acid (HNO₃) and ammonia (NH₃), typical within urban environment, contribute to
495 freshly particles survival by increasing dramatically their growth rate.
496
497 In the afternoon, CS during event days increases due to the growth of freshly emitted particles, especially
498 during summer. Contribution of newly formed particles ($D_p < 50 \text{ nm}$) to the CS is about 36% and 27%,
499 during summer and spring respectively, while the contribution of pre-existing particles ($D_p > 150 \text{ nm}$) to
500 the CS is below 20% for both seasons. Moreover, during non-event days, the size resolved median CS is
501 shifted to larger particle diameters with a maximum observed around 100 nm for all seasons.
502 To evaluate the impact of the background CS on NPF occurrence, all CS values observed from 07:00-
503 09:00, period before NPF starting time (green area on Figure 4a), were averaged during event, non-event
504 and undefined days. It was found that the total CS_{07-09h} was larger (around 16%) during non-event days
505 in comparison to undefined and event days. Moreover, this difference is mostly due to particles larger
506 than 70 nm according to size resolved CS_{07-09h} (Figure 8b). The difference between non-event and event
507 days is lower than what is usually observed over pristine sites (Lyubovtseva et al., 2005) but significant
508 enough to trigger the NPF event occurrence.
509

a supprimé:

a supprimé:

a déplacé vers le haut [2]: (Marten et al., 2022; Wang et al., 2020),

a déplacé (et inséré) [2]

a mis en forme : Couleur de police : Texte 1

a supprimé: %

a supprimé: %

a supprimé: %

a supprimé: %

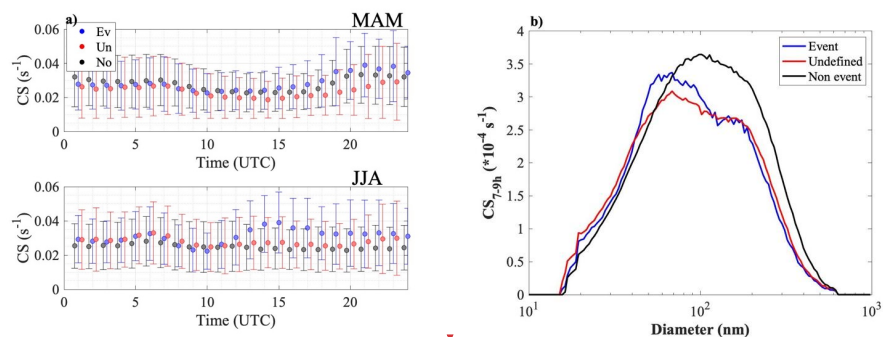
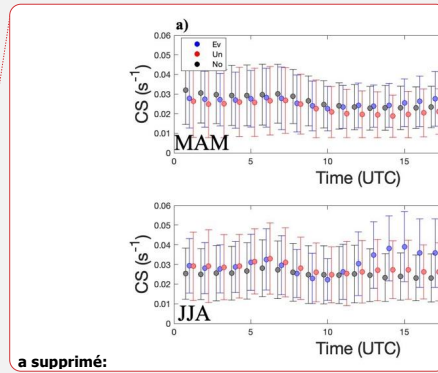


Figure 8 : (a) Diel variation of Condensation Sink (CS) during spring (MAM) and summer (JJA) seasons. (b) Median size resolved CS for MAM and JJA during event days (blue), undefined (red) and non-event days (black).



a supprimé:

a supprimé: %

Additionally, the correlation coefficients between meteorological parameters and pollutants (gas and particles) are reported in Table 1 for the entire period of measurements (all seasons). Hourly average over a time window between 09:00 - 14:00 (NPF event starting time period) of few variables (total CS, T, RH and BC_{wb}) were used to calculate those correlation coefficients (corresponding to 7025 and 35433 data points for NPF event and Non-event days, respectively).

The correlation of Black Carbon from wood burning (BC_{wb}) during non-event days with the condensation sink is high ($R = 0.67$). This correlation between these parameters is clearly absent during event days ($R = 0.19$). One can also note that NO_x concentrations have a positive correlation (0.30) with CS during NPF non-event days while the same correlation is negative (-0.17) during NPF event days. The NO_x sources over urban area are mostly anthropogenic (house heating, traffic and industries) sources which is consistent with its relatively high correlation coefficients with BC_{wb} (0.47 and 0.65). As highlighted in (Barreira et al., 2020), BC_{wb} and NO_x are evolving through the year showing a minimum in summer and a maximum in winter when sources are stronger due to colder temperatures and residential heating emissions. As non-event days are mostly (62%) observed during cold months (fall and winter) and NPF

events are largely (82.%) observed during warmer months (spring and summer), the correlation between BC_{wb}, NO_x and CS during non-event is not surprising. However, during spring, air masses observed during NPF events are clearly “cleaner” (in terms of NO_x and BC_{wb}) than non-event cases. Indeed, NO_x and BC_{wb} concentrations are lowered by 18.% and 36.% respectively during spring NPF event days in comparison to non-event days. During summer, NO_x and BC_{wb} concentrations reach an annual minimum and there both pollutant concentrations are similar between NPF event and non-event days (lowered by - 0.04.% and 0.01.% during NPF event days).

Table 1 : Correlation coefficients between different meteorological parameters (T, RH), Nitrogen oxide (NO_x), Black carbon concentrations (BC_{wb} from wood burning) and total condensation sink during event and non-event for the 4 years period (2017-2020) and in a time window (09:00 – 14:00). High positive or negative correlations are marked in bold.

		CS	T	RH	NO _x	BC _{wb}
Event days	CS	1				
	T	0.55	1			
	RH	-0.39	-0.40	1		
	NO _x	-0.17	-0.24	0.48	1	
	BC _{wb}	0.19	-0.04	0.11	0.47	1
Non- event days	CS	1				
	T	0.06	1			
	RH	-0.03	-0.50	1		
	NO _x	0.30	-0.44	0.44	1	
	BC _{wb}	0.67	-0.37	0.28	0.65	1

Moreover, during event days the temperature is positively correlated (0.55) with the CS, while, during non-event days, this correlation is clearly not observed during non-event days (0.06). Over boreal forest,

554 CS and temperature are correlated during event day (Liao et al., 2014). Indeed, this coupling comes from
555 the enhanced growth of particles due larger monoterpene emissions at higher temperature, which naturally
556 leads to higher concentration of larger particles and thus higher CS. As the particle growth during event
557 days is clearly related to temperature increase (Figure 5) most probably due to higher concentration of
558 condensable gasses, it is not surprising to observe this temperature and CS coupling.

560 **3.6 Air mass trajectories**

561 One can note that environmental conditions (CS, Temperature and RH) observed during undefined events
562 are mostly between event and non-event days. A deeper analysis on undefined days reveals that on these
563 days, particle growth stopped due to (i) a decrease of the total irradiance due to a cloud passage over the
564 site (20.% of cases), (ii) a shift of the wind direction (17.% of cases), (iii) or both parameters changing
565 simultaneously (35.% of cases).

567 The shift of the wind orientation leading to a stop of the particle growth indicates that NPF events are
568 associated with certain wind directions or air mass origins. To investigate this, HYSPLIT back trajectories
569 were first sorted as a function of event, non-event and undefined days. Only the back-trajectories arriving
570 between 09:00-14:00 (period of NPF high occurrences) were selected for further analysis. During the
571 NPF events, the predominant air masses were tracked back along the Eastern North Sea region.
572 Comparing these results to back trajectories during non-event days highlight more continental influence.
573 Indeed, most of the back trajectories during non-event days pass over large cities (Dunkirk, Paris, London,
574 Rotterdam) before reaching Lille metropolis. Those air masses might then have been slightly enriched in
575 pre-existing particles larger than 100 nm (CS_{7.9h} slightly larger (16.% during non-event days) which
576 would decrease the occurrence of NPF events in Lille or could have been depleted in precursor vapors.
577 This result is consistent with previous results showing “cleaner” air masses are associated with NPF event
578 cases observed during spring.

579

a supprimé: %

a supprimé: %

a supprimé: %

a supprimé: %

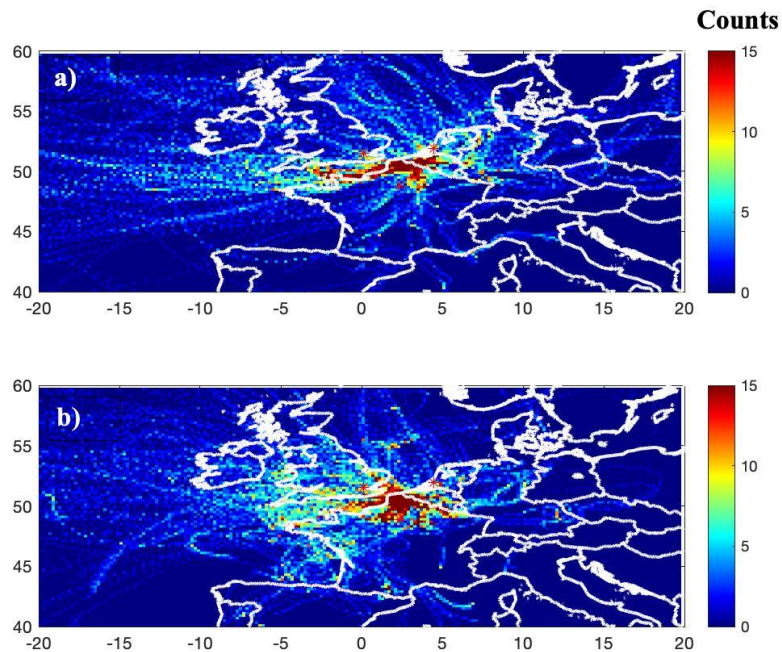


Figure 9 : 3 days hourly back trajectories arriving in ATOLL between 09:00-14:00 UTC during (a) New Particle Formation (NPF) events and (b) non-events days. The back trajectories were calculated for each hour at ATOLL at half the boundary layer height. The color contour represents the back trajectories crossing counts in each grid cell (resolution $0.2^\circ \cdot 0.2^\circ$).

a supprimé: n

a supprimé: p

a supprimé: f

584

585 3.7 Nucleation strength factor

586 The nucleation strength factor ($NSF_{15.7-100}$) is calculated as the ratio of fine to accumulation particle
 587 concentrations observed during nucleation day over the same ratio observed during non-event day (Salma
 588 et al., 2017). Fine and accumulation mode particle number concentrations ($N_{15.7-100}$ and $N_{100-800}$) were

retrieved from the SMPS data. The limited atmospheric residence time of fine particles (typically lower than 10 h) means that a large portion of the $N_{15.7-100}$ concentration can also be related to local emissions and/or formation processes, including NPF events. On the contrary, due to a longer residence time within the atmosphere (up to 10 days), $N_{100-800}$ is more related to large spatial and temporal scales. Therefore, the numerator represents the increase of $N_{<100}$ relative to $N_{100-800}$ caused by all sources while the denominator represents the same property due to all sources except NPF. The NSF method is based on the hypothesis that aerosol sources are similar from day to day and from season to season, excepting the sporadic occurrence of NPF. Considering the large number of event (96) and non-event (432) days used to calculate $NSF_{15.7-100}$, one can assume that the sporadic/occasional (i.e. not observed on daily basis) sources of UF particles other than NPF events (e.g. volcanic plumes) have little impact on the $NSF_{15.7-100}$ in comparison to the sources always active (such as traffic, industries etc...).

NSF is generally used to better assess the contribution of NPF to fine particle number concentrations (represented by $N_{<100}$) relative to the regional background particle number concentrations. If the $NSF \approx 1$, then the relative contribution of NPF to particle number concentration with respect to other sources is negligible, like in Granada (Spain) urban site (Casquero-Vera et al., 2021). Moreover, Salma et al. (2017) also defined two thresholds for NSF_{6-100} to describe NPF contribution as a single source: a considerable contribution ($1 < NSF_{6-100} < 2$) or larger than of any other source sectors together ($NSF_{6-100} > 2$). One should keep in mind that these thresholds were defined accordingly to the lower cut off diameter originally set at 6nm. As the lower cut off diameter used in this study is a bit larger (15.7 nm instead of 6nm) than the one used by Salma et al. (2017), the calculated $NSF_{15.7-100}$ would necessarily be underestimated in comparison to NSF_{6-100} from Salma et al. (2017). The hourly median of fine to accumulation particle concentration ratio was computed for NPF event and non-event days. Figure 10 shows the $NSF_{15.7-100}$ diel variation observed at the ATOLL platform over 4 years of measurements.

During spring, the $NSF_{15.7-100}$ factor remains quite constant (about 1.5) during night and morning and peaks at 16:00 UTC to reach a maximum at 2.5. This indicates that NPF has a significant effect on particle number concentration only a few (2-3) hours after the averaged NPF starting time. During summer, the tendency of the $NSF_{15.7-100}$ is quite similar with a unique peak at 13:00 UTC (again 2-3 hours after the

619 averaged NPF starting time). At that time the median NSF_{15.7-100} values reach 4 while from 21:00 to 06:00
 620 UTC the NSF_{15.7-100} remains low (averaged at 1.08). Therefore, during summer, the NPF contribution to
 621 particle number concentration is extremely high from 10:00 to 18:00 and then negligible for the rest of
 622 the day in comparison to other sources.
 623 Such NSF₁₀₋₁₀₀ diel variations were observed in other European cities (Budapest, Vienna and Prague) with
 624 maximum reaching 2.7, 2.3 and 3.4 respectively with a lower cut-off diameter set at 10nm (Németh et al.,
 625 2018). Moreover, Salma et al. (2017) reported NSF₆₋₁₀₀ peaks at midday varying from 2.2 and 2.7 for
 626 Budapest city center and from 2 to 7.2 for near city background for each season with NSF₆₋₁₀₀ maximum
 627 reached during winter. The nucleation frequency during winter in Budapest is low (<10%), similarly to
 628 our observations, however, the impact of these limited number of events on particle number
 629 concentrations is high. For the record, the NSF_{15.7-100} factor peaked at 3.5 and 2.3 during winter and fall
 630 respectively.

631
 632

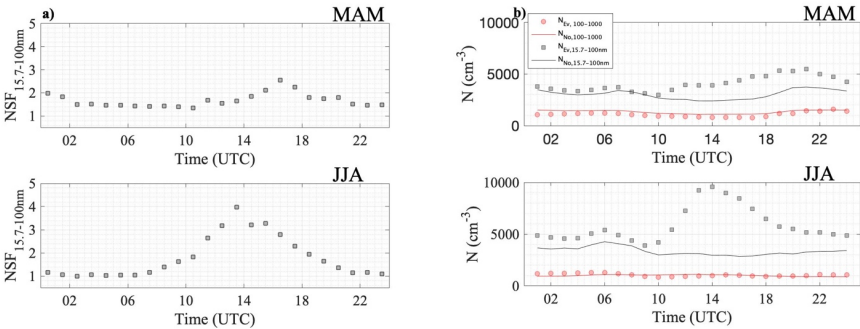
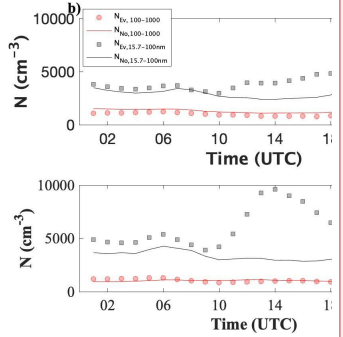
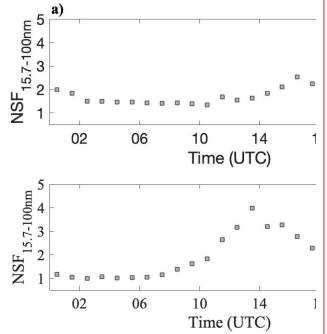


Figure 10 : (a) Diel variation of the Nucleation Strength Factor (NSF_{15.7-100}) during MAM and JJA calculated from number concentration during the 2017-2020 period. (b) Diel variation of particle number concentrations (N) for each season within the diameter ranges from 15.7 to 100 nm (N_{15.7-100}, black) and from 100 to 1000 nm (N₁₀₀₋₁₀₀₀, red) at the ATOLL site during the 2017-2020 period. The dots correspond to event days while the line correspond to non-event days.

a supprimé: %



a supprimé:



a supprimé:

636 4 Conclusions

637 This study was based on 4-years (2017- 2020) measurements performed at the ATOLL site, in the close
638 vicinity of the city of Lille, Northern France. This paper is dedicated to studying New Particle Formation
639 (NPF) occurrence over a peri-urban site. The results highlight a strong seasonal variation of the NPF event
640 frequency, with a maximum occurrence observed during spring (23, %) and summer (26, %). The
641 undefined cases, which correspond to bursts of UFP that do not grow, are much more frequent (38, % on
642 average) than NPF events all year long. The highest frequency (68, %) is observed in August and the
643 lowest one (17, %) in February. The interruption of the particle growth during undefined events can be
644 mostly attributed to changes of environmental conditions (irradiance and wind direction).

645 Seasonal variation of NPF parameters was also clearly observed and associated with environmental
646 parameters. High temperature ($T > 295\text{K}$), low RH ($\text{RH} < 45, \%$) and high solar radiation favor the
647 occurrence of NPF events at ATOLL. The presence of clouds, linked to a decrease of solar radiation, is
648 limiting the NPF event occurrences. Moreover, NPF events start earlier in the morning during from May
649 to September, most probably related to variations in sunrise time. The Growth Rate calculated between
650 15.7 and 30 nm ($\text{GR}_{15.7-30\text{nm}}$) ranges from 1.8 nm.h-1 in March up to 10.9 nm.h-1 in July. The $\text{GR}_{15.7-30\text{nm}}$
651 was also found to be positively correlated with temperature. This correlation might be related to larger
652 emissions of biogenic precursors at higher temperatures, including monoterpenes known to favor the
653 occurrence of NPF event (Kulmala et al., 2004).

654 Relatively high values of Condensation Sink (averaged $\text{CS} > 2.10^{-2} \text{ s}^{-1}$) are reported during NPF events
655 as well as during non-event days. These results suggest that high CS values are not limiting the NPF event
656 occurrence, consistent with recent studies focusing on NPF events over urban sites (Deng et al., 2020;
657 Hussein et al., 2020; Pushpawela et al., 2018). Looking more closely before the NPF onset (from 07:00 –
658 09:00 UTC), $\text{CS}_{07-09\text{h}}$ values are larger by 16, % during non-event days. Interestingly, CS tends to increase
659 during event days (especially in summer) and size resolved CS clearly shows a peak shift from 150 nm
660 during non-event days to 50 nm during event days highlighting the strong contribution of newly formed
661 particles on CS.

a supprimé: n
a supprimé: p
a supprimé: f
a supprimé: %
a supprimé: %
a supprimé: %
a supprimé: %
a supprimé: %

a supprimé: %

a supprimé: warmer months (

a supprimé: -
a supprimé:)
a supprimé: g
a supprimé: r

a supprimé: %

677 Air masses trajectories (HYSPLIT) arriving over ATOLL during event days highlight a specific path
678 along the Eastern North Sea region with only a small fraction passing over any continental area and
679 therefore not crossing many anthropogenic sources, while, most of the back trajectories during non-event
680 days pass over large cities (Dunkirk, Paris, London, Rotterdam) before reaching Lille. The precursor
681 vapor concentration and probably their nature might differ from both “clean” and “polluted” air masses
682 and therefore promote or inhibit NPF event occurrences, a point which requires further investigation.

683
684 The impact of NPF events on particle number concentrations has been estimated through the nucleation
685 strength factor (NSF; Salma et al., 2017). The $NSF_{15.7-100nm}$ diel variation was calculated for spring and
686 summer occurring 2 to 3 hours after the average NPF starting time and reaching 1.5 and 4 during spring
687 and summer respectively. The extremely large $NSF_{15.7-100nm}$ value observed during summer highlights
688 the very high NPF contribution to the fine particles ($D_p < 100$ nm) number concentration in comparison
689 to other regional sources. Recently, (Ren et al., 2021) highlighted the strong impact of newly formed
690 particles from NPF on Cloud Condensation Nuclei (CCN) especially at sites close to anthropogenic
691 sources, such as ATOLL. In future studies, the impact of local vertical dynamics such as the effect of
692 boundary layer dynamics as in Lampilahti et al. (2020 and 2021) as well as the CCN enhancement factor
693 will be analysed.

694

695

696 **Acknowledgements**

697 This research was supported by the French national research agency (ANR) under the MABCaM (ANR-16-CE04-0009)
698 contract. Part of the instrumental system has been financially supported by the CaPPA project (Chemical and Physical
699 Properties of the Atmosphere), which is funded by the French National Research Agency (ANR) through the PIA (Programme
700 d'Investissement d'Avenir) under contract “ANR-11-LABX-0005-01”, and by the Regional Council “Hauts-de-France”. [«This
701 work has benefited from the support of the research infrastructure ACTRIS-FR, registered on the Roadmap of the French
702 Ministry of Research.](#) The authors also thank the Région Hauts-de-France, and the Ministère de l'Enseignement Supérieur et
703 de la Recherche (CPER Climibio), and the European Fund for Regional Economic Development for their financial support.
704 The authors gratefully acknowledge the NOAA Air Resources Laboratory (ARL) for the provision of the HYSPLIT transport

705 and dispersion model and/or READY website (<https://www.ready.noaa.gov>) used in this publication. We thank Francois
706 Thieuleux for ECMWF data sharing during this work.

707

708

709 **Data availability**

710 ATOLL measurements are available through the EBAS database (<https://ebas.nilu.no>) and SMPS data
711 before 2020 through <https://doi.org/10.5281/zenodo.6794562>. GDAS files for back-
712 trajectory calculation are available at <https://www.arl.noaa.gov/hysplit/hysplit/>. NOx data are
713 available from the ATMO open data website : <https://data-atmo-hdf.opendata.arcgis.com>.

714

715

716

717 **References :**

718

719 [Barreira, L.M.F., Helin, A., Aurela, M., Teinilä, K., Friman, M., Kangas, L., Niemi, J.V., Portin, H.,](#)
720 [Kousa, A., Pirjola, L., Rönkkö, T., Saarikoski, S., Timonen, H., 2020. In-depth characterization of](#)
721 [submicron particulate matter inter-annual variations at a street canyon site in Northern Europe \(preprint\).](#)
722 [Aerosols/Field Measurements/Troposphere/Chemistry \(chemical composition and reactions\).](#)
723 <https://doi.org/10.5194/acp-2020-908>
724 [Berland, K., Rose, C., Pey, J., Culot, A., Freney, E., Kalivitis, N., Kouvarakis, G., Cerro, J.C., Mallet, M.,](#)
725 [Sartelet, K., Beckmann, M., Bourriane, T., Roberts, G., Marchand, N., Mihalopoulos, N., Sellegri, K.,](#)
726 [2017. Spatial extent of new particle formation events over the Mediterranean Basin from multiple ground-](#)
727 [based and airborne measurements. Atmospheric Chem. Phys. 17, 9567–9583.](#)
728 <https://doi.org/10.5194/acp-17-9567-2017>
729 [Boichu, M., Favez, O., Riffault, V., Petit, J.-E., Zhang, Y., Brogniez, C., Sciare, J., Chiapello, I., Clarisse,](#)
730 [L., Zhang, S., Pujol-Söhne, N., Tison, E., Delbarre, H., Goloub, P., 2019. Large-scale particulate air](#)

Code de champ modifié

Code de champ modifié

Code de champ modifié

a mis en forme : Anglais (E.U.)

731 pollution and chemical fingerprint of volcanic sulfate aerosols from the 2014–2015 Holuhraun flood lava
 732 eruption of Bárðarbunga volcano (Iceland). *Atmospheric Chem. Phys.* 19, 14253–14287.
 733 <https://doi.org/10.5194/acp-19-14253-2019>
 734 Bousiotis, D., Brean, J., Pope, F.D., Dall’Osto, M., Querol, X., Alastuey, A., Perez, N., Petäjä, T.,
 735 Massling, A., Nøjgaard, J.K., Nordstrøm, C., Kouvarakis, G., Vratolis, S., Eleftheriadis, K., Niemi, J.V.,
 736 Portin, H., Wiedensohler, A., Weinhold, K., Merkel, M., Tuch, T., Harrison, R.M., 2021. The effect of
 737 meteorological conditions and atmospheric composition in the occurrence and development of new
 738 particle formation (NPF) events in Europe. *Atmospheric Chem. Phys.* 21, 3345–3370.
 739 <https://doi.org/10.5194/acp-21-3345-2021>
 740 Bovchaliuk, V., Goloub, P., Podvin, T., Veselovskii, I., Tanre, D., Chaikovsky, A., Dubovik, O., Mortier,
 741 A., Lopatin, A., Korenskiy, M., Victori, S., 2016. Comparison of aerosol properties retrieved using
 742 GARRLiC, LIRIC, and Raman algorithms applied to multi-wavelength lidar and sun/sky-photometer
 743 data. *Atmos Meas Tech* 9, 3391–3405. <https://doi.org/10.5194/amt-9-3391-2016>
 744 Boy, M., Kulmala, M., 2002. Influence of spectral solar irradiance on the formation of new particles in
 745 the continental boundary layer (preprint). <https://doi.org/10.5194/acpd-2-1317-2002>
 746 Casquero-Vera, J.A., Lyamani, H., Titos, G., Minguión, M.C., Dada, L., Alastuey, A., Querol, X.,
 747 Petäjä, T., Olmo, F.J., Alados-Arboledas, L., 2021. Quantifying traffic, biomass burning and secondary
 748 source contributions to atmospheric particle number concentrations at urban and suburban sites. *Sci. Total*
 749 *Environ.* 768, 145282. <https://doi.org/10.1016/j.scitotenv.2021.145282>
 750 Chen, G., Canonaco, F., Tobler, A., Aas, W., Alastuey, A., Allan, J., Atabakhsh, S., Aurela, M.,
 751 Baltensperger, U., Bougiatioti, A., De Brito, J.F., Ceburnis, D., Chazeau, B., Chebaicheb, H.,
 752 Daellenbach, K.R., Ehn, M., El Haddad, I., Eleftheriadis, K., Favez, O., Flentje, H., Font, A., Fossum, K.,
 753 Frenay, E., Gini, M., Green, D.C., Heikkinen, L., Herrmann, H., Kalogridis, A.-C., Keernik, H., Lhotka,
 754 R., Lin, C., Lunder, C., Maasikmets, M., Manousakas, M.I., Marchand, N., Marin, C., Marmureanu, L.,
 755 Mihalopoulos, N., Močnik, G., Nęcki, J., O’Dowd, C., Ovadnevaite, J., Peter, T., Petit, J.-E., Pikridas,
 756 M., Matthew Platt, S., Pokorná, P., Poulain, L., Priestman, M., Riffault, V., Rinaldi, M., Rózański, K.,
 757 Schwarz, J., Sciare, J., Simon, L., Skiba, A., Slowik, J.G., Sosedova, Y., Stavroulas, I., Styszko, K.,
 758 Teinmaa, E., Timonen, H., Tremper, A., Vasilescu, J., Via, M., Vodička, P., Wiedensohler, A., Zografou,

O., Cruz Minguillón, M., Prévôt, A.S.H., 2022. European Aerosol Phenomenology - 8: Harmonised Source Apportionment of Organic Aerosol using 22 Year-long ACSM/AMS Datasets. *Environ. Int.* 107325. <https://doi.org/10.1016/j.envint.2022.107325>

Clifford, S., Mazaheri, M., Salimi, F., Ezz, W.N., Yeganeh, B., Low-Choy, S., Walker, K., Mengersen, K., Marks, G.B., Morawska, L., 2018. Effects of exposure to ambient ultrafine particles on respiratory health and systemic inflammation in children. *Environ. Int.* 114, 167–180. <https://doi.org/10.1016/j.envint.2018.02.019>

Cuesta-Mosquera, A., Močnik, G., Drinovec, L., Müller, T., Pfeifer, S., Minguillón, M., Björn, B., Buckley, P., Dudoitis, V., Fernández-García, J., Fernández Amado, M., Brito, J., Flentje, H., Heffernan, E., Kalivitis, N., Kalogridis, C., Keernik, H., Marmureanu, L., Luoma, K., Wiedensohler, A., 2020. Intercomparison and characterization of 23 Aethalometers under laboratory and ambient air conditions: Procedures and unit-to-unit variabilities. <https://doi.org/10.5194/amt-2020-344>

Dada, L., Paasonen, P., Nieminen, T., Buenrostro Mazon, S., Kontkanen, J., Peräkylä, O., Lehtipalo, K., Hussein, T., Petäjä, T., Kerminen, V.-M., Bäck, J., Kulmala, M., 2017. Long-term analysis of clear-sky new particle formation events and nonevents in Hyytiälä. *Atmospheric Chem. Phys.* 17, 6227–6241. <https://doi.org/10.5194/acp-17-6227-2017>

Dal Maso, M., Kulmala, M., Riipinen, I., Wagner, R., Hussein, T., Aalto, P.P., Lehtinen, K.E.J., 2005. Formation and growth of fresh atmospheric aerosols: Eight years of aerosol size distribution data from SMEAR II, Hyytiälä, Finland. *Boreal Environ. Res.* 10, 323–336.

Dall'Osto, M., Beddows, D.C.S., Asmi, A., Poulain, L., Hao, L., Freney, E., Allan, J.D., Canagaratna, M., Crippa, M., Bianchi, F., de Leeuw, G., Eriksson, A., Swietlicki, E., Hansson, H.C., Henzing, J.S., Granier, C., Zemankova, K., Laj, P., Onasch, T., Prevot, A., Putaud, J.P., Sellegri, K., Vidal, M., Virtanen, A., Simo, R., Worsnop, D., O'Dowd, C., Kulmala, M., Harrison, R.M., 2018. Novel insights on new particle formation derived from a pan-european observing system. *Sci. Rep.* 8, 1482. <https://doi.org/10.1038/s41598-017-17343-9>

Deng, C., Fu, Y., Dada, L., Yan, C., Cai, R., Yang, D., Zhou, Y., Yin, R., Lu, Y., Li, X., Qiao, X., Fan, X., Nie, W., Kontkanen, J., Kangasluoma, J., Chu, B., Ding, A., Kerminen, V.-M., Paasonen, P., Worsnop, D.R., Bianchi, F., Liu, Y., Zheng, J., Wang, L., Kulmala, M., Jiang, J., 2020. Seasonal

787 Characteristics of New Particle Formation and Growth in Urban Beijing. *Environ. Sci. Technol.* 54, 8547–
788 8557. <https://doi.org/10.1021/acs.est.0c00808>

789 Dos Santos, V.N., Herrmann, E., Manninen, H.E., Hussein, T., Hakala, J., Nieminen, T., Aalto, P.P.,
790 Merkel, M., Wiedensohler, A., Kulmala, M., Petäjä, T., Hämeri, K., 2015. Variability of air ion
791 concentrations in urban Paris. *Atmospheric Chem. Phys.* 15, 13717–13737. [https://doi.org/10.5194/acp-](https://doi.org/10.5194/acp-15-13717-2015)
792 15-13717-2015

793 Duplissy, J., Merikanto, J., Franchin, A., Tsagkogeorgas, G., Kangasluoma, J., Wimmer, D., Vuollekoski,
794 H., Schobesberger, S., Lehtipalo, K., Flagan, R.C., Brus, D., Donahue, N.M., Vehkamäki, H., Almeida,
795 J., Amorim, A., Barmet, P., Bianchi, F., Breitenlechner, M., Dunne, E.M., Guida, R., Henschel, H.,
796 Junninen, H., Kirkby, J., Kürten, A., Kupc, A., Määttänen, A., Makhmutov, V., Mathot, S., Nieminen, T.,
797 Onnela, A., Praplan, A.P., Riccobono, F., Rondo, L., Steiner, G., Tome, A., Walther, H., Baltensperger,
798 U., Carslaw, K.S., Dommen, J., Hansel, A., Petäjä, T., Sipilä, M., Stratmann, F., Vrtala, A., Wagner, P.E.,
799 Worsnop, D.R., Curtius, J., Kulmala, M., 2016. Effect of ions on sulfuric acid-water binary particle
800 formation: 2. Experimental data and comparison with QC-normalized classical nucleation theory:
801 BINARY PARTICLE FORMATION EXPERIMENTS. *J. Geophys. Res. Atmospheres* 121, 1752–1775.
802 <https://doi.org/10.1002/2015JD023539>

803 Fuks, N.A., Sutugin, A.G., 1970. *Highly Dispersed Aerosols*. Ann Arbor Science Publishers.

804 Größ, J., Hamed, A., Sonntag, A., Spindler, G., Manninen, H.E., Nieminen, T., Kulmala, M., Hörrak, U.,
805 Plass-Dülmer, C., Wiedensohler, A., Birmili, W., 2018. Atmospheric new particle formation at the
806 research station Melpitz, Germany: connection with gaseous precursors and meteorological parameters.
807 *Atmospheric Chem. Phys.* 18, 1835–1861. <https://doi.org/10.5194/acp-18-1835-2018>

808 Hamed, A., Korhonen, H., Sihto, S.-L., Joutsensaari, J., Järvinen, H., Petäjä, T., Arnold, F., Nieminen,
809 T., Kulmala, M., Smith, J.N., Lehtinen, K.E.J., Laaksonen, A., 2011. The role of relative humidity in
810 continental new particle formation. *J. Geophys. Res.* 116, D03202.
811 <https://doi.org/10.1029/2010JD014186>

812 Heinritzi, M., Dada, L., Simon, M., Stolzenburg, D., Wagner, A.C., Fischer, L., Ahonen, L.R.,
813 Amanatidis, S., Baalbaki, R., Baccarini, A., Bauer, P.S., Baumgartner, B., Bianchi, F., Brilke, S., Chen,
814 D., Chiu, R., Dias, A., Dommen, J., Duplissy, J., Finkenzeller, H., Frege, C., Fuchs, C., Garmash, O.,

§15 Gordon, H., Granzin, M., El Haddad, I., He, X., Helm, J., Hofbauer, V., Hoyle, C.R., Kangasluoma, J.,
 §16 Keber, T., Kim, C., Kürten, A., Lamkaddam, H., Laurila, T.M., Lampilahti, J., Lee, C.P., Lehtipalo, K.,
 §17 Leiminger, M., Mai, H., Makhmutov, V., Manninen, H.E., Marten, R., Mathot, S., Mauldin, R.L.,
 §18 Mentler, B., Molteni, U., Müller, T., Nie, W., Nieminen, T., Onnela, A., Partoll, E., Passananti, M., Petäjä,
 §19 T., Pfeifer, J., Pospisilova, V., Quéléver, L.L.J., Rissanen, M.P., Rose, C., Schobesberger, S., Scholz, W.,
 §20 Scholze, K., Sipilä, M., Steiner, G., Stozhkov, Y., Tauber, C., Tham, Y.J., Vazquez-Pufleau, M., Virtanen,
 §21 A., Vogel, A.L., Volkamer, R., Wagner, R., Wang, M., Weitz, L., Wimmer, D., Xiao, M., Yan, C., Ye,
 §22 P., Zha, Q., Zhou, X., Amorim, A., Baltensperger, U., Hansel, A., Kulmala, M., Tomé, A., Winkler, P.M.,
 §23 Worsnop, D.R., Donahue, N.M., Kirkby, J., Curtius, J., 2020. Molecular understanding of the suppression
 §24 of new-particle formation by isoprene. *Atmospheric Chem. Phys.* 20, 11809–11821.
 §25 <https://doi.org/10.5194/acp-20-11809-2020>
 §26 Jokinen, V., Mäkelä, J.M., 1997. Closed-loop arrangement with critical orifice for DMA sheath/excess
 §27 flow system. *J. Aerosol Sci.* 28, 643–648. [https://doi.org/10.1016/S0021-8502\(96\)00457-0](https://doi.org/10.1016/S0021-8502(96)00457-0)
 §28 Kalkavouras, P., Bossioli, E., Bezantakos, S., Bougiatioti, A., Kalivitis, N., Stavroulas, I., Kouvarakis,
 §29 G., Protonotariou, A.P., Dandou, A., Biskos, G., Mihalopoulos, N., Nenes, A., Tombrou, M., 2017. New
 §30 particle formation in the southern Aegean Sea during the Etesians: importance for CCN production and
 §31 cloud droplet number. *Atmospheric Chem. Phys.* 17, 175–192. <https://doi.org/10.5194/acp-17-175-2017>
 §32 Kanawade, V.P., Sebastian, M., Hooda, R.K., Hyvärinen, A.-P., 2022. Atmospheric new particle
 §33 formation in India: Current understanding and knowledge gaps. *Atmos. Environ.* 270, 118894.
 §34 <https://doi.org/10.1016/j.atmosenv.2021.118894>
 §35 Kerminen, V.-M., Chen, X., Vakkari, V., Petäjä, T., Kulmala, M., Bianchi, F., 2018. Atmospheric new
 §36 particle formation and growth: review of field observations. *Environ. Res. Lett.* 13, 103003.
 §37 <https://doi.org/10.1088/1748-9326/aadf3c>
 §38 Kerminen, V.-M., Pirjola, L., Kulmala, M., 2001. How significantly does coagulation scavenging limit
 §39 atmospheric particle production? *J. Geophys. Res. Atmospheres* 106, 24119–24125.
 §40 <https://doi.org/10.1029/2001JD000322>
 §41 Kontkanen, J., Lehtipalo, K., Ahonen, L., Kangasluoma, J., Manninen, H.E., Hakala, J., Rose, C., Sellegri,
 §42 K., Xiao, S., Wang, L., Qi, X., Nie, W., Ding, A., Yu, H., Lee, S., Kerminen, V.-M., Petäjä, T., Kulmala,

a mis en forme : Anglais (E.U.)

a mis en forme : Anglais (E.U.)

§43 M., 2017. Measurements of sub-3 nm particles using a particle size magnifier in different environments:
 §44 from clean mountain top to polluted megacities. *Atmospheric Chem. Phys.* 17, 2163–2187.
 §45 <https://doi.org/10.5194/acp-17-2163-2017>
 §46 Kulmala, M., 2003. Atmospheric science. How particles nucleate and grow. *Science* 302, 1000–1001.
 §47 <https://doi.org/10.1126/science.1090848>
 §48 Kulmala, M., Dal Maso, M., Mäkelä, J.M., Pirjola, L., Väkevä, M., Aalto, P., Mikkulainen, P., Hämeri,
 §49 K., O'Dowd, C.D., 2001. On the formation, growth and composition of nucleation mode particles. *Tellus*
 §50 *Ser. B Chem. Phys. Meteorol.* 53, 479–490. <https://doi.org/10.1034/j.1600-0889.2001.530411.x>
 §51 Kulmala, M., Kerminen, V.-M., Petäjä, T., Ding, A.J., Wang, L., 2017. Atmospheric gas-to-particle
 §52 conversion: why NPF events are observed in megacities? *Faraday Discuss.* 200, 271–288.
 §53 <https://doi.org/10.1039/C6FD00257A>
 §54 Kulmala, M., Petäjä, T., Ehn, M., Thornton, J., Sipilä, M., Worsnop, D.R., Kerminen, V.-M., 2014.
 §55 Chemistry of Atmospheric Nucleation: On the Recent Advances on Precursor Characterization and
 §56 Atmospheric Cluster Composition in Connection with Atmospheric New Particle Formation. *Annu. Rev.*
 §57 *Phys. Chem.* 65, 21–37. <https://doi.org/10.1146/annurev-physchem-040412-110014>
 §58 Kulmala, M., Petäjä, T., Nieminen, T., Sipilä, M., Manninen, H.E., Lehtipalo, K., Maso, M.D., Aalto,
 §59 P.P., Junninen, H., Paasonen, P., Riipinen, I., Lehtinen, K.E.J., Laaksonen, A., Kerminen, V.M., 2012.
 §60 Measurement of the nucleation of atmospheric aerosol particles. *Nat. Protoc.* 7, 1651–1667.
 §61 <https://doi.org/10.1038/nprot.2012.091>
 §62 Kulmala, M., Vehkamäki, H., Petäjä, T., Dal Maso, M., Lauri, A., Kerminen, V.-M., Birmili, W.,
 §63 McMurry, P.H., 2004. Formation and growth rates of ultrafine atmospheric particles: a review of
 §64 observations. *J. Aerosol Sci.* 35, 143–176. <https://doi.org/10.1016/j.jaerosci.2003.10.003>
 §65 Kurtén, T., Torpo, L., Ding, C.-G., Vehkamäki, H., Sundberg, M.R., Laasonen, K., Kulmala, M., 2007.
 §66 A density functional study on water-sulfuric acid-ammonia clusters and implications for atmospheric
 §67 cluster formation. *J. Geophys. Res. Atmospheres* 112. <https://doi.org/10.1029/2006JD007391>
 §68 Laj, P., Bigi, A., Rose, C., Andrews, E., Lund Myhre, C., Collaud Coen, M., Lin, Y., Wiedensohler, A.,
 §69 Schulz, M., Ogren, J.A., Fiebig, M., Gliß, J., Mortier, A., Pandolfi, M., Petäjä, T., Kim, S.-W., Aas, W.,
 §70 Putaud, J.-P., Mayol-Bracero, O., Keywood, M., Labrador, L., Aalto, P., Ahlberg, E., Alados Arboledas,

871 L., Alastuey, A., Andrade, M., Artíñano, B., Ausmeel, S., Arsov, T., Asmi, E., Backman, J.,
 872 Baltensperger, U., Bastian, S., Bath, O., Beukes, J.P., Brem, B.T., Bukowiecki, N., Conil, S., Couret, C.,
 873 Day, D., Dayantolis, W., Degorska, A., Eleftheriadis, K., Fetfatzis, P., Favez, O., Flentje, H., Gini, M.I.,
 874 Gregorič, A., Gysel-Beer, M., Hallar, A.G., Hand, J., Hoffer, A., Hueglin, C., Hooda, R.K., Hyvärinen,
 875 A., Kalapov, I., Kalivitis, N., Kasper-Giebl, A., Kim, J.E., Kouvarakis, G., Kranjc, I., Krejci, R., Kulmala,
 876 M., Labuschagne, C., Lee, H.-J., Lihavainen, H., Lin, N.-H., Löschau, G., Luoma, K., Marinoni, A.,
 877 Martins Dos Santos, S., Meinhardt, F., Merkel, M., Metzger, J.-M., Mihalopoulos, N., Nguyen, N.A.,
 878 Ondracek, J., Pérez, N., Perrone, M.R., Petit, J.-E., Picard, D., Pichon, J.-M., Pont, V., Prats, N., Prenni,
 879 A., Reisen, F., Romano, S., Sellegri, K., Sharma, S., Schauer, G., Sheridan, P., Sherman, J.P., Schütze,
 880 M., Schwerin, A., Sohmer, R., Sorribas, M., Steinbacher, M., Sun, J., Titos, G., Toczko, B., Tuch, T.,
 881 Tulet, P., Tunved, P., Vakkari, V., Velarde, F., Velasquez, P., Villani, P., Vratolis, S., Wang, S.-H.,
 882 Weinhold, K., Weller, R., Yela, M., Yus-Diez, J., Zdimal, V., Zieger, P., Zikova, N., 2020. A global
 883 analysis of climate-relevant aerosol properties retrieved from the network of Global Atmosphere Watch
 884 (GAW) near-surface observatories. *Atmospheric Meas. Tech.* 13, 4353–4392.
 885 <https://doi.org/10.5194/amt-13-4353-2020>
 886 Liao, L., Kerminen, V.-M., Boy, M., Kulmala, M., Dal Maso, M., 2014. Temperature influence on the
 887 natural aerosol budget over boreal forests. *Atmospheric Chem. Phys.* 14, 8295–8308.
 888 <https://doi.org/10.5194/acp-14-8295-2014>
 889 Lyubovtseva, Y.S., Sogacheva, L., Maso, M.D., Bonn, B., Keronen, P., Kulmala, M., 2005. Seasonal
 890 variations of trace gases, meteorological parameters, and formation of aerosols in boreal forests 10, 18.
 891 Marten, R., Xiao, M., Rörup, B., Wang, M., Kong, W., He, X.-C., Stolzenburg, D., Pfeifer, J., Marie, G.,
 892 Wang, D.S., Scholz, W., Baccarini, A., Lee, C.P., Amorim, A., Baalbaki, R., Bell, D.M., Bertozzi, B.,
 893 Caudillo, L., Chu, B., Dada, L., Duplissy, J., Finkenzeller, H., Carracedo, L.G., Granzin, M., Hansel, A.,
 894 Heinritzi, M., Hofbauer, V., Kempainen, D., Kürten, A., Lampimäki, M., Lehtipalo, K., Makhmutov,
 895 V., Manninen, H.E., Mentler, B., Petäjä, T., Philippov, M., Shen, J., Simon, M., Stozhkov, Y., Tomé, A.,
 896 Wagner, A.C., Wang, Y., Weber, S.K., Wu, Y., Zauner-Wieczorek, M., Curtius, J., Kulmala, M., Möhler,
 897 O., Volkamer, R., Winkler, P.M., Worsnop, D.R., Dommen, J., Flagan, R.C., Kirkby, J., Donahue, N.M.,
 898 Lamkaddam, H., Baltensperger, U., Haddad, I.E., 2022. Survival of newly formed particles in haze

conditions. *Environ. Sci. Atmospheres* 2, 491–499. <https://doi.org/10.1039/D2EA00007E>

Mazon, S.B., Riipinen, I., Schultz, D.M., Valtanen, M., Maso, M.D., Sogacheva, L., Junninen, H., Nieminen, T., 2009. Classifying previously undefined days from eleven years of aerosol-particle-size distribution data from the SMEAR II station, Hyytiälä, Finland. *Atmos Chem Phys* 10.

Merikanto, J., Duplissy, J., Määttänen, A., Henschel, H., Donahue, N.M., Brus, D., Schobesberger, S., Kulmala, M., Vehkamäki, H., 2016. Effect of ions on sulfuric acid-water binary particle formation: 1. Theory for kinetic- and nucleation-type particle formation and atmospheric implications: BINARY PARTICLE FORMATION THEORY. *J. Geophys. Res. Atmospheres* 121, 1736–1751. <https://doi.org/10.1002/2015JD023538>

Mortier, A., Goloub, P., Podvin, T., Deroo, C., Chaikovsky, A., Ajtai, N., Blarel, L., Tanre, D., Derimian, Y., 2013. Detection and characterization of volcanic ash plumes over Lille during the Eyjafjallajökull eruption. *Atmos Chem Phys* 13, 3705–3720. <https://doi.org/10.5194/acp-13-3705-2013>

Németh, Z., Rosati, B., Zíková, N., Salma, I., Bozó, L., Dameto de España, C., Schwarz, J., Ždímal, V., Wonaschütz, A., 2018. Comparison of atmospheric new particle formation events in three Central European cities. *Atmos. Environ.* 178, 191–197. <https://doi.org/10.1016/j.atmosenv.2018.01.035>

Nieminen, T., Kerminen, V.-M., Petäjä, T., Aalto, P.P., Arshinov, M., Asmi, E., Baltensperger, U., Beddows, D.C.S., Beukes, J.P., Collins, D., Ding, A., Harrison, R.M., Henzing, B., Hooda, R., Hu, M., Hörrak, U., Kivekäs, N., Komsaare, K., Krejci, R., Kristensson, A., Laakso, L., Laaksonen, A., Leaitch, W.R., Lihavainen, H., Mihalopoulos, N., Németh, Z., Nie, W., O'Dowd, C., Salma, I., Sellegri, K., Svenningsson, B., Swietlicki, E., Tunved, P., Ulevicius, V., Vakkari, V., Vana, M., Wiedensohler, A., Wu, Z., Virtanen, A., Kulmala, M., 2018. Global analysis of continental boundary layer new particle formation based on long-term measurements. *Atmospheric Chem. Phys.* 18, 14737–14756. <https://doi.org/10.5194/acp-18-14737-2018>

Ohlwein, S., Kappeler, R., Kutlar Joss, M., Künzli, N., Hoffmann, B., 2019. Health effects of ultrafine particles: a systematic literature review update of epidemiological evidence. *Int. J. Public Health* 64, 547–559. <https://doi.org/10.1007/s00038-019-01202-7>

Paasonen, P., Peltola, M., Kontkanen, J., Junninen, H., Kerminen, V.-M., Kulmala, M., 2018. Comprehensive analysis of particle growth rates from nucleation mode to cloud condensation nuclei in

a mis en forme : Anglais (E.U.)

boreal forest. *Atmospheric Chem. Phys.* 18, 12085–12103. <https://doi.org/10.5194/acp-18-12085-2018>

Peng, Y., Dong, Y., Li, X., Liu, X., Dai, J., Chen, C., Dong, Z., Du, C., Wang, Z., 2017. Different Characteristics of New Particle Formation Events at Two Suburban Sites in Northern China. *Atmosphere* 8, 258. <https://doi.org/10.3390/atmos8120258>

Pierce, J.R., Adams, P.J., 2009. Uncertainty in global CCN concentrations from uncertain aerosol nucleation and primary emission rates. *Atmospheric Chem. Phys.* 9, 1339–1356. <https://doi.org/10.5194/acp-9-1339-2009>

Ren, J., Chen, L., Fan, T., Liu, J., Jiang, S., Zhang, F., 2021. The NPF Effect on CCN Number Concentrations: A Review and Re-Evaluation of Observations From 35 Sites Worldwide. *Geophys. Res. Lett.* 48, e2021GL095190. <https://doi.org/10.1029/2021GL095190>

Rodríguez, S., Cuevas, E., González, Y., Ramos, R., Romero, P.M., Pérez, N., Querol, X., Alastuey, A., 2008. Influence of sea breeze circulation and road traffic emissions on the relationship between particle number, black carbon, PM₁, PM_{2.5} and PM_{2.5}–10 concentrations in a coastal city. *Atmos. Environ.* 42, 6523–6534. <https://doi.org/10.1016/j.atmosenv.2008.04.022>

Rodríguez, S., Van Dingenen, R., Putaud, J.-P., Martins-Dos Santos, S., Roselli, D., 2005. Nucleation and growth of new particles in the rural atmosphere of Northern Italy—relationship to air quality monitoring. *Atmos. Environ.* 39, 6734–6746. <https://doi.org/10.1016/j.atmosenv.2005.07.036>

Roig Rodelas, R., Chakraborty, A., Perdrix, E., Tison, E., Riffault, V., 2019. Real-time assessment of wintertime organic aerosol characteristics and sources at a suburban site in northern France. *Atmos. Environ.* 203, 48–61. <https://doi.org/10.1016/j.atmosenv.2019.01.035>

Rolph, G., Stein, A., Stunder, B., 2017. Real-time Environmental Applications and Display sYstem: READY. *Environ. Model. Softw.* 95, 210–228. <https://doi.org/10.1016/j.envsoft.2017.06.025>

Rose, C., Collaud Coen, M., Andrews, E., Lin, Y., Bossert, I., Lund Myhre, C., Tuch, T., Wiedensohler, A., Fiebig, M., Aalto, P., Alastuey, A., Alonso-Blanco, E., Andrade, M., Artíñano, B., Arsov, T., Baltensperger, U., Bastian, S., Bath, O., Beukes, J.P., Brem, B.T., Bukowiecki, N., Casquero-Vera, J.A., Conil, S., Eleftheriadis, K., Favez, O., Flentje, H., Gini, M.I., Gómez-Moreno, F.J., Gysel-Beer, M., Hallar, A.G., Kalapov, I., Kalivitis, N., Kasper-Giebl, A., Keywood, M., Kim, J.E., Kim, S.-W., Kristensson, A., Kulmala, M., Lihavainen, H., Lin, N.-H., Lyamani, H., Marinoni, A., Martins Dos

a mis en forme : Anglais (E.U.)

a mis en forme : Anglais (E.U.)

a mis en forme : Anglais (E.U.)

955 Santos, S., Mayol-Bracero, O.L., Meinhardt, F., Merkel, M., Metzger, J.-M., Mihalopoulos, N., Ondracek,
 956 J., Pandolfi, M., Pérez, N., Petäjä, T., Petit, J.-E., Picard, D., Pichon, J.-M., Pont, V., Putaud, J.-P., Reisen,
 957 F., Sellegri, K., Sharma, S., Schauer, G., Sheridan, P., Sherman, J.P., Schwerin, A., Sohmer, R., Sorribas,
 958 M., Sun, J., Tulet, P., Vakkari, V., van Zyl, P.G., Velarde, F., Villani, P., Vratolis, S., Wagner, Z., Wang,
 959 S.-H., Weinhold, K., Weller, R., Yela, M., Zdimal, V., Laj, P., 2021. Seasonality of the particle number
 960 concentration and size distribution: a global analysis retrieved from the network of Global Atmosphere
 961 Watch (GAW) near-surface observatories. *Atmospheric Chem. Phys.* 21, 17185–17223.
 962 <https://doi.org/10.5194/acp-21-17185-2021>
 963 Rose, C., Sellegri, K., Asmi, E., Hervo, M., Freney, E., Colomb, A., Junninen, H., Duplissy, J., Sipilä,
 964 M., Kontkanen, J., Lehtipalo, K., Kulmala, M., 2015a. Major contribution of neutral clusters to new
 965 particle formation at the interface between the boundary layer and the free troposphere. *Atmospheric*
 966 *Chem. Phys.* 15, 3413–3428. <https://doi.org/10.5194/acp-15-3413-2015>
 967 Rose, C., Sellegri, K., Freney, E., Dupuy, R., Colomb, A., Pichon, J.-M., Ribeiro, M., Bourianne, T.,
 968 Burnet, F., Schwarzenboeck, A., 2015b. Airborne measurements of new particle formation in the free
 969 troposphere above the Mediterranean Sea during the HYMEX campaign. *Atmospheric Chem. Phys.* 15,
 970 10203–10218. <https://doi.org/10.5194/acp-15-10203-2015>
 971 Rose, C., Sellegri, K., Moreno, I., Velarde, F., Ramonet, M., Weinhold, K., Krejci, R., Andrade, M.,
 972 Wiedensohler, A., Ginot, P., Laj, P., 2017. CCN production by new particle formation in the free
 973 troposphere. *Atmospheric Chem. Phys.* 17, 1529–1541. <https://doi.org/10.5194/acp-17-1529-2017>
 974 Salimi, F., Rahman, M.M., Clifford, S., Ristovski, Z., Morawska, L., 2017. Nocturnal new particle
 975 formation events in urban environments. *Atmospheric Chem. Phys.* 17, 521–530.
 976 <https://doi.org/10.5194/acp-17-521-2017>
 977 Salma, I., Németh, Z., Kerminen, V.-M., Aalto, P., Nieminen, T., Weidinger, T., Molnár, Á., Imre, K.,
 978 Kulmala, M., 2016. Regional effect on urban atmospheric nucleation. *Atmospheric Chem. Phys.* 16,
 979 8715–8728. <https://doi.org/10.5194/acp-16-8715-2016>
 980 Sandradewi, J., Prévôt, A.S.H., Szidat, S., Perron, N., Alfarra, M.R., Lanz, V.A., Weingartner, E.,
 981 Baltensperger, U., 2008. Using aerosol light absorption measurements for the quantitative determination
 982 of wood burning and traffic emission contributions to particulate matter. *Environ. Sci. Technol.* 42, 3316–

983 3323.

984 Sellegri, K., Rose, C., Marinoni, A., Lupi, A., Wiedensohler, A., Andrade, M., Bonasoni, P., Laj, P., 2019.

985 New Particle Formation: A Review of Ground-Based Observations at Mountain Research Stations.

986 *Atmosphere* 10, 493. <https://doi.org/10.3390/atmos10090493>

987 Shukla, K.K., Niranjana Kumar, K., Phanikumar, D.V., Newsom, R.K., Kotamarthi, V.R., Ouarda,

988 T.B.M.J., Ratnam, M.V., 2016. Identification of the cloud base height over the central Himalayan region:

989 Intercomparison of Ceilometer and Doppler Lidar (preprint). *Clouds/Remote Sensing/Validation and*

990 *Intercomparisons*. <https://doi.org/10.5194/amt-2016-162>

991 Sogacheva, L., Hamed, A., Facchini, M.C., Kulmala, M., Laaksonen, A., 2007. Relation of air mass

992 history to nucleation events in Po Valley, Italy, using back trajectories analysis. *Atmos Chem Phys* 15.

993 Sogacheva, L., Maso, M.D., Kerminen, V.M., Kulmala, M., 2005. Probability of nucleation events and

994 aerosol particle concentration in different air mass types arriving at Hyytiälä southern Finland, based on

995 back trajectories analysis. *Boreal Environ. Res.* 10, 479–491.

996 Spracklen, D.V., Carslaw, K.S., Kulmala, M., Kerminen, V.-M., Mann, G.W., Sihto, S.-L., 2006. The

997 contribution of boundary layer nucleation events to total particle concentrations on regional and global

998 scales. *Atmospheric Chem. Phys.* 6, 5631–5648. <https://doi.org/10.5194/acp-6-5631-2006>

999 Stein, A.F., Draxler, R.R., Rolph, G.D., Stunder, B.J.B., Cohen, M.D., Ngan, F., 2015. NOAA's

000 HYSPLIT Atmospheric Transport and Dispersion Modeling System. *Bull. Am. Meteorol. Soc.* 96, 2059–

001 2077. <https://doi.org/10.1175/BAMS-D-14-00110.1>

002 Tuch, T.M., Herbarth, O., Franck, U., Peters, A., Wehner, B., Wiedensohler, A., Heintzenberg, J., 2006.

003 Weak correlation of ultrafine aerosol particle concentrations <800 nm between two sites within one city.

004 *J. Expo. Sci. Environ. Epidemiol.* 16, 486–490. <https://doi.org/10.1038/sj.jes.7500469>

005 Tunved, P., Hansson, H.-C., Kerminen, V.-M., Ström, J., Dal Maso, M., Lihavainen, H., Viisanen, Y.,

006 Aalto, P.P., Komppula, M., Kulmala, M., 2006. High natural aerosol loading over boreal forests. *Science*

007 312, 261–263. <https://doi.org/10.1126/science.1123052>

008 Villani, P., Picard, D., Marchand, N., Laj, P., 2007. Design and validation of a 6-volatility tandem

009 differential mobility analyzer (VTDMA). *Aerosol Sci. Technol.* 41, 898–906.

010 <https://doi.org/10.1080/02786820701534593>

a mis en forme : Anglais (E.U.)

a mis en forme : Anglais (E.U.)

011 Wang, M., Kong, W., Marten, R., He, X.-C., Chen, D., Pfeifer, J., Heitto, A., Kontkanen, J., Dada, L.,
 012 Kürten, A., Yli-Juuti, T., Manninen, H.E., Amanatidis, S., Amorim, A., Baalbaki, R., Baccarini, A., Bell,
 013 D.M., Bertozzi, B., Bräkling, S., Brilke, S., Murillo, L.C., Chiu, R., Chu, B., De Menezes, L.-P., Duplissy,
 014 J., Finkenzeller, H., Carracedo, L.G., Granzin, M., Guida, R., Hansel, A., Hofbauer, V., Krechmer, J.,
 015 Lehtipalo, K., Lamkaddam, H., Lampimäki, M., Lee, C.P., Makhmutov, V., Marie, G., Mathot, S.,
 016 Mauldin, R.L., Mentler, B., Müller, T., Onnela, A., Partoll, E., Petäjä, T., Philippov, M., Pospisilova, V.,
 017 Ranjithkumar, A., Rissanen, M., Rörup, B., Scholz, W., Shen, J., Simon, M., Sipilä, M., Steiner, G.,
 018 Stolzenburg, D., Tham, Y.J., Tomé, A., Wagner, A.C., Wang, D.S., Wang, Y., Weber, S.K., Winkler,
 019 P.M., Wlasits, P.J., Wu, Y., Xiao, M., Ye, Q., Zauner-Wieczorek, M., Zhou, X., Volkamer, R., Riipinen,
 020 I., Dommen, J., Curtius, J., Baltensperger, U., Kulmala, M., Worsnop, D.R., Kirkby, J., Seinfeld, J.H.,
 021 El-Haddad, I., Flagan, R.C., Donahue, N.M., 2020. Rapid growth of new atmospheric particles by nitric
 022 acid and ammonia condensation. *Nature* 581, 184–189. <https://doi.org/10.1038/s41586-020-2270-4>
 023 Wang, Z., Wu, Z., Yue, D., Shang, D., Guo, S., Sun, J., Ding, A., Wang, L., Jiang, J., Guo, H., Gao, J.,
 024 Cheung, H.C., Morawska, L., Keywood, M., Hu, M., 2017. New particle formation in China: Current
 025 knowledge and further directions. *Sci. Total Environ.* 577, 258–266.
 026 <https://doi.org/10.1016/j.scitotenv.2016.10.177>
 027 Wang, Z.B., Hu, M., Wu, Z.J., Yue, D.L., Zheng, J., Zhang, R.Y., Pei, X.Y., Paasonen, P., Dal Maso, M.,
 028 Boy, M., Wiedensohler, A., 2013. Investigation of the connections between atmospheric new particle
 029 formation and organics at an urban site of Beijing (preprint). *Aerosols/Field*
 030 *Measurements/Troposphere/Chemistry* (chemical composition and reactions).
 031 <https://doi.org/10.5194/acpd-13-3419-2013>
 032 Wehner, B., Wiedensohler, A., 2003. Long term measurements of submicrometer urban aerosols:
 033 statistical analysis for correlations with meteorological conditions and trace gases. *Atmospheric Chem.*
 034 *Phys.* 3, 867–879. <https://doi.org/10.5194/acp-3-867-2003>
 035 Xiao, S., Wang, M.Y., Yao, L., Kulmala, M., Zhou, B., Yang, X., Chen, J.M., Wang, D.F., Fu, Q.Y.,
 036 Worsnop, D.R., Wang, L., 2015. Strong atmospheric new particle formation in winter in urban Shanghai,
 037 China. *Atmospheric Chem. Phys.* 15, 1769–1781. <https://doi.org/10.5194/acp-15-1769-2015>
 038 Yao, L., Garmash, O., Bianchi, F., Zheng, J., Yan, C., Kontkanen, J., Junninen, H., Mazon, S.B., Ehn,

039 M., Paasonen, P., Sipilä, M., Wang, M., Wang, X., Xiao, S., Chen, H., Lu, Y., Zhang, B., Wang, D., Fu,
040 Q., Geng, F., Li, L., Wang, H., Qiao, L., Yang, X., Chen, J., Kerminen, V.-M., Petäjä, T., Worsnop, D.R.,
041 Kulmala, M., Wang, L., 2018. Atmospheric new particle formation from sulfuric acid and amines in a
042 Chinese megacity. *Science* 361, 278–281. <https://doi.org/10.1126/science.aao4839>
043 Yli-Juuti, T., Nieminen, T., Hirsikko, A., Aalto, P.P., Asmi, E., Hörrak, U., Manninen, H.E., Patokoski,
044 J., Dal Maso, M., Petäjä, T., Rinne, J., Kulmala, M., Riipinen, I., 2011. Growth rates of nucleation mode
045 particles in Hyytiälä during 2003–2009: variation with particle size, season, data analysis method and
046 ambient conditions. *Atmospheric Chem. Phys.* 11, 12865–12886. [https://doi.org/10.5194/acp-11-12865-](https://doi.org/10.5194/acp-11-12865-2011)
047 2011

048

049

▼
▲
Page 6 : [1] a supprimé Microsoft Office User 02/09/2022 17:39:00

▼
▲
Page 6 : [1] a supprimé Microsoft Office User 02/09/2022 17:39:00

▼
▲
Page 6 : [2] a mis en forme Microsoft Office User 22/08/2022 10:11:00

Police :Gras

▲
Page 6 : [2] a mis en forme Microsoft Office User 22/08/2022 10:11:00

Police :Gras

▲
Page 6 : [2] a mis en forme Microsoft Office User 22/08/2022 10:11:00

Police :Gras

▲
Page 6 : [2] a mis en forme Microsoft Office User 22/08/2022 10:11:00

Police :Gras

▲
Page 6 : [2] a mis en forme Microsoft Office User 22/08/2022 10:11:00

Police :Gras

▲
Page 6 : [2] a mis en forme Microsoft Office User 22/08/2022 10:11:00

Police :Gras

▲
Page 6 : [2] a mis en forme Microsoft Office User 22/08/2022 10:11:00

Police :Gras

▲
Page 6 : [2] a mis en forme Microsoft Office User 22/08/2022 10:11:00

Police :Gras

▲
Page 6 : [2] a mis en forme Microsoft Office User 22/08/2022 10:11:00

Police :Gras

▲
Page 6 : [3] a supprimé Microsoft Office User 19/08/2022 10:27:00

▼
▲
Page 6 : [3] a supprimé Microsoft Office User 19/08/2022 10:27:00

▼
▲

▲
Page 6 : [4] a supprimé Microsoft Office User 22/08/2022 10:18:00

▼
▲
Page 6 : [4] a supprimé Microsoft Office User 22/08/2022 10:18:00

▼
▲
Page 6 : [4] a supprimé Microsoft Office User 22/08/2022 10:18:00

▼
▲
Page 6 : [4] a supprimé Microsoft Office User 22/08/2022 10:18:00

▼
▲
Page 6 : [4] a supprimé Microsoft Office User 22/08/2022 10:18:00

▼
▲
Page 6 : [4] a supprimé Microsoft Office User 22/08/2022 10:18:00

▼
▲
Page 6 : [4] a supprimé Microsoft Office User 22/08/2022 10:18:00

▼
▲
Page 6 : [5] a mis en forme Microsoft Office User 22/08/2022 10:11:00

Police :12 pt

▲
Page 6 : [5] a mis en forme Microsoft Office User 22/08/2022 10:11:00

Police :12 pt

▲
Page 6 : [5] a mis en forme Microsoft Office User 22/08/2022 10:11:00

Police :12 pt

▲
Page 6 : [5] a mis en forme Microsoft Office User 22/08/2022 10:11:00

Police :12 pt

▲
Page 6 : [5] a mis en forme Microsoft Office User 22/08/2022 10:11:00

Police :12 pt

▲
Page 6 : [5] a mis en forme Microsoft Office User 22/08/2022 10:11:00

Police :12 pt

▲
Page 6 : [5] a mis en forme Microsoft Office User 22/08/2022 10:11:00

Police :12 pt

▲
Page 6 : [6] a mis en forme Microsoft Office User 22/08/2022 10:40:00

Police :12 pt

▲
Page 6 : [6] a mis en forme Microsoft Office User 22/08/2022 10:40:00

Police :12 pt

▲
Page 6 : [6] a mis en forme Microsoft Office User 22/08/2022 10:40:00

Police :12 pt

▲
Page 6 : [6] a mis en forme Microsoft Office User 22/08/2022 10:40:00

Police :12 pt

▲
Page 6 : [6] a mis en forme Microsoft Office User 22/08/2022 10:40:00

Police :12 pt

▲
Page 6 : [6] a mis en forme Microsoft Office User 22/08/2022 10:40:00

Police :12 pt

▲
Page 6 : [6] a mis en forme Microsoft Office User 22/08/2022 10:40:00

Police :12 pt

▲
Page 6 : [6] a mis en forme Microsoft Office User 22/08/2022 10:40:00

Police :12 pt

▲
Page 6 : [6] a mis en forme Microsoft Office User 22/08/2022 10:40:00

Police :12 pt

▲
Page 6 : [6] a mis en forme Microsoft Office User 22/08/2022 10:40:00

Police :12 pt

▲
Page 6 : [6] a mis en forme Microsoft Office User 22/08/2022 10:40:00

Police :12 pt

▲
Page 6 : [6] a mis en forme Microsoft Office User 22/08/2022 10:40:00

Police :12 pt

▲
Page 6 : [6] a mis en forme Microsoft Office User 22/08/2022 10:40:00

Police :12 pt

▲
Page 6 : [6] a mis en forme Microsoft Office User 22/08/2022 10:40:00

Police :12 pt

▲
Page 15 : [7] a supprimé Microsoft Office User 22/08/2022 13:34:00
▼